Supporting Information

Insights into the Synthesis of NHC-Stablized Au Nanoclusters Through Real-Time Reaction Monitoring

Junliang Liu,[+a] Yusuke Sato,[+a] Viveka K. Kulkarni,[b,c] Angus I. Sullivan,[b,c] Wenyu Zhang,[a] Cathleen M. Crudden[*bcd] and Jason E. Hein[*a]

[a] Department of Chemistry, The University of British Columbia, Vancouver, BC V6T 1Z1, Canada

[b] Department of Chemistry, 90 Bader Lane, Queen's University, Kingston, ON, K7L 3N6, Canada

[c] Carbon to Metals Coating Institute–C2MCI, Queen's University, Kingston, ON, K7L 3N6, Canada

[d] Institute of Transformative Bio-Molecules (WPI-ITbM), Nagoya University, Nagoya 464-8602, Japan

*Email for J. E. H.: jhein@chem.ubc.ca

*Email for C. M. C.: cruddenc@chem.queensu.ca

Table of Contents

S1. General information

All reagents and solvents were purchased from Millipore Sigma, Oakwood and Alfa Aesar, and used as received. 1,3-dibenzyl-*1H*-benzo[*d*]imidazol-3-ium chloride, (1,3-dibenzyl-1*H*-benzo[*d*]imidazol-2-ylidene) gold(I) chloride (**1**), (1,3-dibenzyl-[2-^{13}C]-1*H*-benzo[*d*]imidazol-2-ylidene) gold(I) chloride and (1,3-dibenzyl-1*H*-benzo[*d*]imidazol-2-ylidene)(pyridin-2-yl)gold tetrafluoroborate (**2**) were synthesized according to literature procedures.[1,2] $[Au_{13}(NHC)_9Cl_3]Cl_2$ (**4**) and $[Au_{24}(NHC)_{14}Cl_2H_3](BF_4)_3$ (**5**) were both synthesized according to literature procedures.[1,2] Optima-grade UHPLC solvents were purchased from Fisher. High-resolution mass spectrometry (HRMS) data were acquired by the UBC Department of Chemistry Mass Spectrometry Center. The Liquid Chromatography (LC) samples were analyzed by HPLC/MS conducted on an Agilent 1200 HPLC. HPLC data were acquired and formatted with OpenLAB ChemStation LC software.

^{1}H, and ^{13}C{^{1}H} spectra were recorded on Bruker AV500 or Bruker AV700 spectrometers and referenced to residual solvent signals and are quoted relative to tetramethylsilane.[3] ^{13}C NMR spectra were recorded at room temperature unless otherwise specified. Experiments at 0 °C were also performed. All NMR data were processed and displayed using MestReNova software. In cases of residual solvent contamination of NMR solvents, these contaminants are noted on each spectrum. Electrospray ionization mass spectra (ESI-MS) of small molecules were recorded at Queen's University using a Thermo Fisher Orbitrap Velos Pro mass spectrometer with a heated-electrospray ionization probe.

S2. Analytical methods

S2.1. HPLC methods

Table S 1. HPLC method for separation development using acetonitrile and formic acid as modifier

Column:	EC-C18 2.7 µm, 3.0 x 50 mm	
Column Temperature:	35 °C	
Flow Rate:	0.65 mL/min	
Detection:	290 nm and 310 nm	
Acquisition Time:	8.0 min run time 4.0 min post run time	
Mobile Phase:	Solvent A = Water with 0.1% formic acid Solvent B = Acetonitrile	
Mobile Phase Program:	Time 0.00 min 8.00 min	B% 50 100
Injection Volume:	3 µL	

Table S 2. HPLC method for separation development using methanol and formic acid as modifier

Column:	EC-C18 2.7 µm, 3.0 x 50 mm	
Column Temperature:	35 °C	
Flow Rate:	0.65 mL/min	
Detection:	290 nm and 310 nm	
Acquisition Time:	8.0 min run time 4.0 min post run time	
Mobile Phase:	Solvent A = Water with 0.1% formic acid Solvent B = Methanol	
Mobile Phase Program:	Time 0.00 min 8.00 min	B% 50 100
Injection Volume:	3 µL	

Table S 3. HPLC method for separation development using methanol and TFA as modifier

Column:	EC-C18 2.7 µm, 3.0 x 50 mm
Column Temperature:	35 °C
Flow Rate:	0.65 mL/min
Detection:	290 nm and 310 nm
Acquisition Time:	8.0 min run time 4.0 min post run time

Mobile Phase:	Solvent A = Water with 0.1% TFA Solvent B = Methanal with 0.1% TFA	
Mobile Phase Program:	Time 0.00 min 8.00 min	B% 50 100
Injection Volume:	3 µL	

Table S 4. HPLC method for reaction monitoring

Column:	EC-C18 2.7 µm, 3.0 x 50 mm	
Column Temperature:	35 °C	
Flow Rate:	0.45 mL/min	
Detection:	210-360 nm	
Acquisition Time:	12.0 min run time 4.0 min post run time	
Mobile Phase:	Solvent A = Water with 0.1% TFA Solvent B = Methanal with 0.1% TFA	
Mobile Phase Program:	Time 0.00 min 8.00 min 12.00 min	B% 50 100 100
Injection Volume:	3 µL	

Table S 5. HPLC method for resolution tests, calibration curve and slow dose experiments

Column:	Two sequentially linked EC-C18 2.7 µm, 3.0 x 50 mm for calibration curve and slow dose experiments. These were used in series to allow for maxial phase variation testing. Ultimately the added theoretical plates provided by this configuration were selected as it provided an improvement to peak shape and resolution, but still required deconvolution.	
Column Temperature:	35 °C	
Flow Rate:	0.65 mL/min	
Detection:	210-360 nm	
Acquisition Time:	12.0 min run time 4.0 min post run time	
Mobile Phase:	Solvent A = Water with 0.1% TFA Solvent B = Methanal with 0.1% TFA	
Mobile Phase Program:	Time 0.00 min 8.00 min	B% 50 100

	12.00 min	100
Injection Volume:	1 μL	

S2.2. MS methods

Table S 6 MS method used in this research

Spray chamber	
Method of spray chamber:	API-ES
Drying gas flow (l/min)	11.0 -13.0
Nebulizer pressure (psig)	35-60
Drying gas temperature (°C)	350
Capillary voltage (V)	3000
MSD signal settings	
Signal 1	Positive, Scan
Mass range	200 - 3000
Threshold	150
Speed (u/sec)	3467
Signal 2	Positive, Scan
Mass range	2500 - 3000
Threshold	150
Speed (u/sec)	1040

S2.3. Column effects on resolution

The resolution among the peaks within the "medium region" was deemed to be insufficient. To tackle this issue, we experimented with various columns and combinations thereof to explore potential improvements in resolution. A solution of species **4** was prepared in DCM at 1 mL volume, to which we added 8μL of a 100 mM NaBH4 solution. This reaction mixture was promptly injected into the HPLC system to assess the resulting resolution from the different columns. Resolution was evaluated based on the two closest peaks appearing in the medium region of the chromatograph. The resolution value was computed using the following equation:

$$Rs = \frac{RT_1 - RT_2}{0.5(W_1 + W_2)}$$

Rs is the resolution.

RT1 is the retention time of the first peak.

RT2 is the retention time of the second peak.

W1 is the width of the first peak at its base.

W2 is the width of the second peak at its base.

The result was listed in **Table S7**:

Table S 7 Tested resolution resulted from various of reverse-phase columns

Entry	Column	Solvents	Rs value	Note
1	EC-C18 2.7 μm 50 mm	Water(0.5% TFA)/ MeOH(0.5%TFA)	1.1129	Column used for main analysis and all reaction profiling
2	EC-CN 2.7 μm 50mm	Water(0.5% TFA)/ MeOH(0.5%TFA)	n.a.	Column blocking, column may decompose or NHC retained in column.
3	Phenyl-Hexyl 2.1 μm 50mm	Water(0.5% TFA)/ MeOH(0.5%TFA)	n.a.	Column blocking, column may decompose or NHC retained in column.

4	SB-C18 2.1 µm 100mm	Water(0.5% TFA)/ MeOH(0.5%TFA)	1.0010	n.a
5	SB-aq 2.7 µm 50 mm	Water(0.5% TFA)/ MeOH(0.5%TFA)	<1.0000	n.a
6	SB-C8 100mm	Water(0.5% TFA)/ MeOH(0.5%TFA)	<1.0000	n.a
7	Phenomex 1.9uM 50mm	Water(0.5% TFA)/ MeOH(0.5%TFA)	<1.0000	n.a.
8	EC-C18 2.7uM + Phenomex 1.9uM 50mm	Water(0.5% TFA)/ MeOH(0.5%TFA)	n.a	Too high pressure (>1100bar with 0.4mL/min flow rate)
9	2x EC-C18 2.7uM 50 + 50mm	Water(0.5% TFA)/ MeOH(0.5%TFA)	1.3417	Slightly improved resolution

Our testing showed that entry 9, involving the combination of two EC-C18 columns, offered marginally improved resolution compared to the method used in entry 1 (which was utilized for reaction monitoring in the primary research). However, all tests resulted in Rs values below 1.5, a benchmark for considering peaks as well-separated. This implies that modifying the column does not significantly enhance the resolution of peaks in the medium region. To address this, we opted to utilize a computational approach[4] (for details see Section **S2.4**) to delineate the overlapping peaks in the medium region, instead of physically separating them through HPLC. This approach allows us to effectively analyze the complex data despite the low resolution.

S2.4. HPLC chromatograph peak deconvoluting algorithum

The peak convolution process starts with detecting overlapped peak groups followed by assigning linear baseline and performing peak deconvolution on each overlapped area. The data analysis pipeline is capable of performing peak deconvolution without peak assignment or manual baseline correction.

Python libraries

Numpy and SciPy are used during peak deconvolution

Function	**Purpose**
scipy.signal.savgol_filter	Smooth raw data
numpy.gradient	Find second derivative
scipy.signal.find_peaks	Find peak from second derivative
scipy.signal.peak_widths	Find peak width for overlapping detection
scipy.optimize.curve_fit	Peak fitting
numpy.trapz	Calculate peak area

Tuning parameters (optional)

Parameter	**Description**	**Default**
range_of_interest	Trim the chromatograph (e.g. [1,5] for range from 1 to 5 min)	None
smooth_window	Number of data point for fitting the polynomial when smoothing	41
peak_height	Threshold that peak above this value in second derivative will be identified	0.05
tailing_fronting	Select the asymmetrical shape to be either tailing or fronting	tailing
peak_width	Restrict the maximum peak width (gaussian)	0.05
smooth_derivative	Whether smooth the derivative to ignore small peaks or noise	False

Processing steps:

Peak identification

The raw HPLC data was smoothed by applying the Savitzky–Golay filter, which involves fitting a polynomial function over adjacent data points. In this peak deconvolution process, a fixed second-order polynomial fitting was employed, and the smooth window length was adjustable. Peak identification was completed by analyzing the second derivatives of the original chromatograph, allowing the detection of hidden shoulder peaks that might not be apparent during direct peak finding. Additionally, the peak height was also adjustable, enabling the fine-tuning of the peak finding.

Overlapping detection

Detected peaks were grouped if the difference of their elution times was within 30 seconds. To estimate the approximate start and end times of each peak, a preliminary baseline fitting and peak deconvolution was applied. In cases where false grouping occurred, and there was no overlapping, the groups were separated and their purities were assessed accordingly.

Peak deconvolution

The peak shape observed in HPLC chromatograms are typically asymmetrical with either tailing or fronting. To accurately model the tailing effect, the exponentially modified Gaussian (EMG) function proves to be the most suitable among various fitting functions. To accommodate both tailing and fronting effects in asymmetric peak fitting, the bi-directional EMG below was utilized.

f = (a0 / 2 / a3 * np.exp(a2 ** 2 / 2.0 / a3 ** 2 + (a1 - t) / a3)

* (erf((t - a1) / (np.sqrt(2.0) * a2) - a2 / np.sqrt(2.0) / a3) + abs(a3) / a3))

a0 is the peak area.

a1 is the elution time.

a2 is the gaussian width parameter.

a3 is the exponential factor.

During the fitting process, the parameters (a0 - a3) of each asymmetrical peak (fi) within the overlapped peak area were treated as independent parameters, and the overall function is represented as the summation of all asymmetrical peak functions. To perform the fitting, the 'scipy.optimize.curve_fit' method was employed, fitting all a0 - a3 parameters of the overall function to the original HPLC chromatogram. This process aimed to obtain the best fit for the EMG function and accurately characterize the peaks' shapes and features in the chromatogram data.

Baseline correction and final fitting

The baseline was determined individually for each overlapped peaks group by connecting the local minimum before the left-most peak and the local minimum after the right-most peak. This baseline correction is essential to establish a zero-baseline for accurate peak deconvolution. During this step, the final retention time and peak area of each identified peak are calculated and reported.

Multiple HPLC data analysis

To investigate the trend of peak areas with respect to retention times over time, peak analysis was performed on all HPLC chromatograms. An offset value (e.g. 0.01 minute) was provided for handling potential retention time shifts during grouping. Peaks with retention times within this threshold were grouped together, facilitating the observation of changes in peak areas over time. The offset value is adjustable, which can adapt to varying experimental conditions and enhance the accuracy of tracking peak variations over time.

Code availability

https://gitlab.com/heingroup/hplc_peak_deconvolution

S2.5. Calibration curves for 1 and 2

To confirm the linearity of the response of our HPLC system with regard to the Au-NHC species, we generated a calibration curve for the starting materials [Au-NHC][Cl] (**1**) and [NHC-Au-Py][BF_4] (**2**). These calibration curves are depicted in Figures **S1** and **S2**. This linear response is critical for ensuring the accuracy of our measurements and the validity of our subsequent analysis.

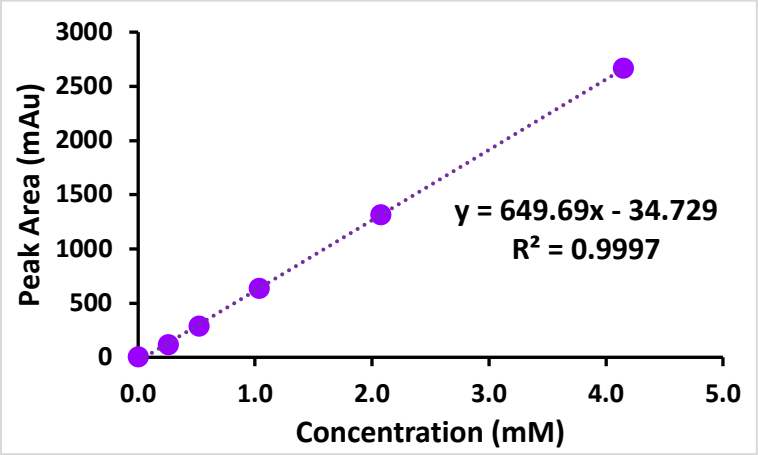

Figure S 1 Calibration curve of [Au-NHC][Cl] (**1**) dissoved in DCM.

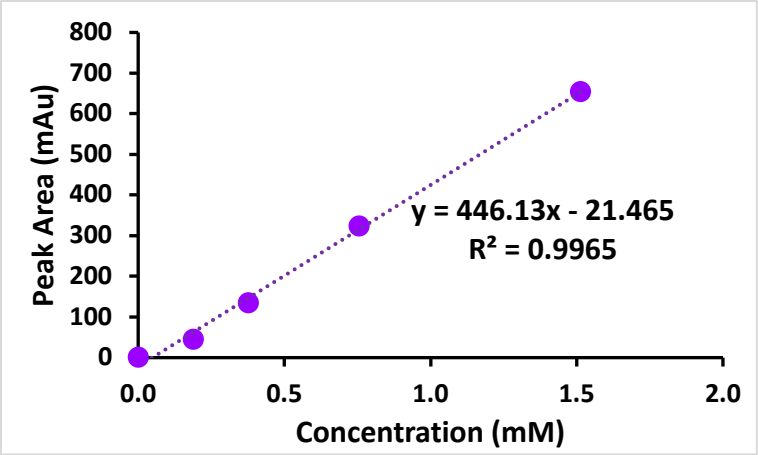

Figure S 2 Calibration curve of [NHC-Au-Py][BF_4] (**2**) dissoved in DCM.

S3. Synthesis and reaction monitoring procedures

S3.1. Synthesis of starting materials

S3.1.1. *N,N*'-Dibenzylbenzimidazolium hexafluorophosphate

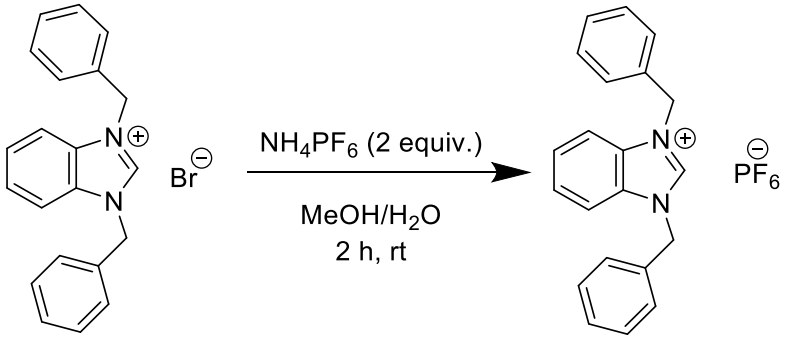

Synthesis of the hexafluorophosphate NHC salt was based on a previously reported similar anion exchange reaction.[5] 1,3-Dibenzyl-1*H*-benzo[*d*]imidazolium bromide (116 mg, 0.3 mmol) was dissolved in 10 mL of H_2O in a 20 mL vial. NH_4PF_6 (100 mg, 0.6 mmol) was dissolved in 30 mL of H_2O in a 100 mL round bottom flask. To the ammonium hexafluorophosphate solution, the NHC salt was added dropwise causing immediate precipitation of a white solid. The mixture was stirred for 2 h and then filtered over a fine porosity frit. The solid was washed with 60 mL of water followed by 60 mL of ether. The solid product was scraped out with a spatula and characterized by NMR spectroscopy (0.1009 g, 74 % yield).^{1}H NMR, ^{13}NMR, and ESI-MS results matched published data.[6]

S3.1.2. Bis(1,3-dibenzyl-1*H*-benzo[*d*]imidazol-2-ylidene)gold(I) hexafluorophosphate (3)

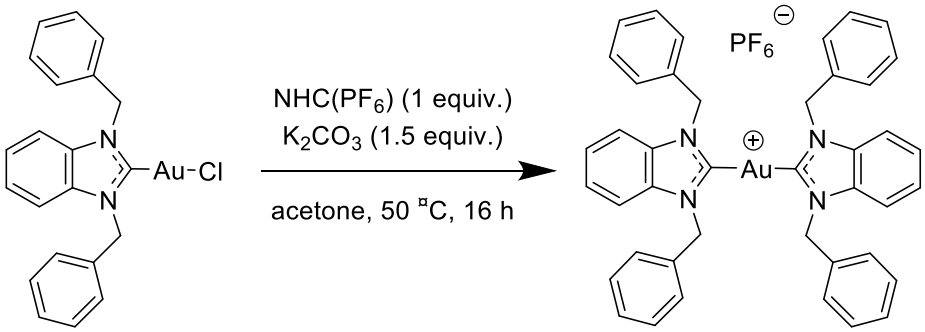

Synthesis of the hexafluorophosphate bis-NHC-Au complex was based on previously reported procedures.[7] 1,3-Dibenzyl-1*H*-benzo[*d*]imidazolium hexafluorphosphate (27 mg, 0.04 mmol) was dissolved in 15 mL acetone in a pressure vessel. (1,3-Dibenzyl-1*H*-benzo[*d*]imidazol-2-ylidene)gold(I) chloride (25 mg, 0.04 mmol) and potassium carbonate (8 mg, 0.06 mmol) were added to solution. The reaction was heated to 50 C and stired overnight, after which time the reaction had turned yellow. The solution was filtered through a silica plug and dried under vacuum to afford a white solid (26 mg, 66% yield). ESI-MS calc'd 793.26, found 793.26. ^{13}C {^{1}H} NMR) δ: 52.3, 112.2, 125.5, 126.8, 128.2, 129.1, 129.5, 133.5, 134.8, 190.9. ^{1}H NMR δ: 5.70 (8H, s, CH_2), 7.25 (8H, d, *Ar*), 7.29-7.35 (12H, m, *Ar*), 7.45-7.52 (8H, m, *Ar*).

S3.2. Reaction monitoring procedure

S3.2.1. $[Au_{13}(NHC)_9Cl_3]Cl_2$ (4) synthesis and monitoring procedure

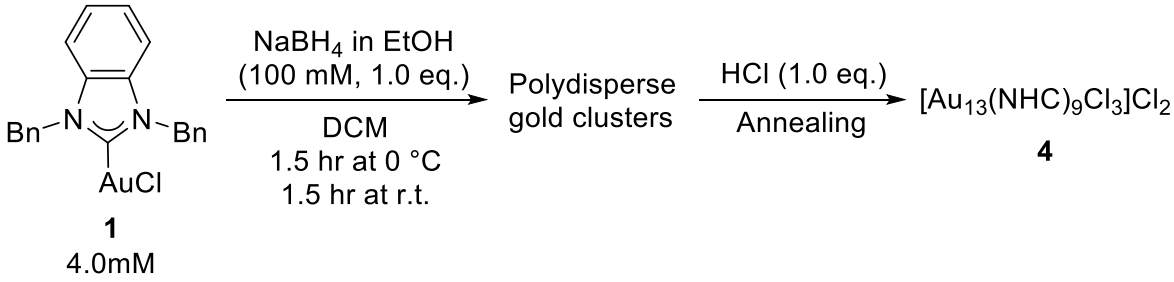

In an HPLC vial, under air, **1** (2.12 mg, 4 μmol) was dissolved in DCM (1.0 mL), and the solution was cooled in an ice-cold water bath for ca. 10 min. This HPLC vial was sampled by an Agilent HPLC/MS with a 15 min time interval during the following steps for reaction monitoring. In another flask, prepare 5 mL of 100 mM $NaBH_4$ (18.9 mg) in ethanol. The $NaBH_4$ in EtOH solution (40 μL, 1 eq.) was added into the **1** solution in one portion, and the solution was mixed well by hand. The solution was left at 0 °C for 1.5 h and then at r.t. for 1.5 h. Concentrated hydrochloric acid (12 M, 0.33 μL, 1 eq.) was added, and the reaction was monitored for 1 h., after which the solution changed color from dark brown to clear orange.

S3.2.2. $[Au_{13}(NHC)_9Cl_3]Cl_2$ (4) synthesis by sequential dose of $NaBH_4$ and monitoring procedure

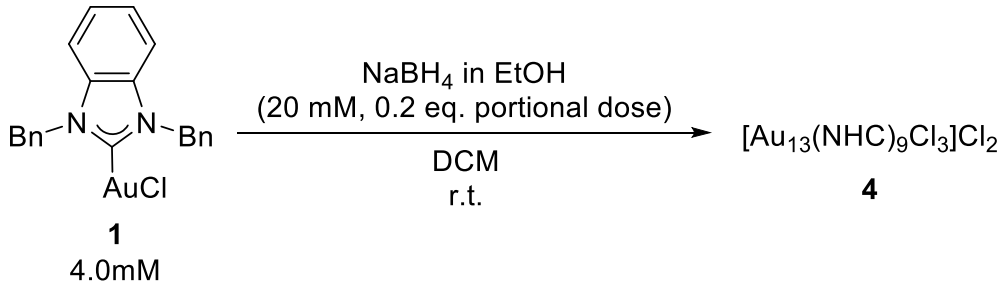

In an HPLC vial, under air, **1** (2.12 mg, 4.0 μmol) was dissolved in DCM (1.0 mL), and the solution was cooled in an ice-cold water bath for ca. 10 min. This HPLC vial was sampled by an Agilent HPLC/MS with 15 min time interval during the following steps for reaction monitoring. In another flask, prepare 15 mL of 20 mM $NaBH_4$ (11.4 mg) in ethanol. The $NaBH_4$ in ethanol solution (40 uL, 0.20 eq.) was added into the **1** solution 0.2 equivalents and monitored for 30-45 minutes. Repeated the addition of 0.2 eq. $NaBH_4$ solution until 1.0 equivalent was added.

S3.2.3. $[Au_{24}(NHC)_{14}Cl_2H_3][BF_4]_3$ (5) synthesis monitoring procedure

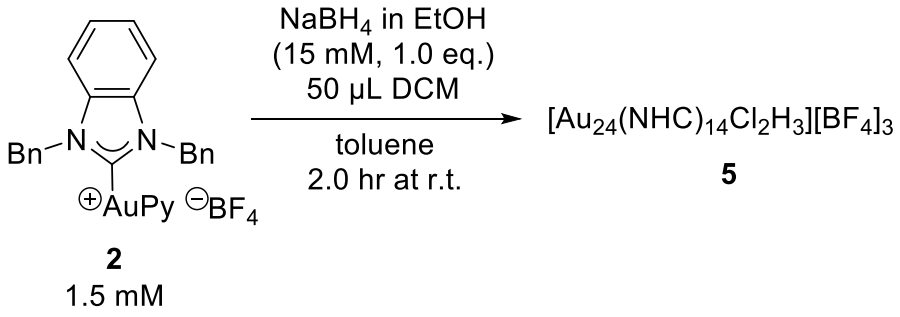

In an HPLC vial, [NHC-Au-Py][BF_4] (**2)** (1.0 mg, 1.5 µmol) was dissolved in toluene (1.0 mL) and cooled to 0 °C. This HPLC vial was sampled by an Agilent HPLC/MS with 15 min time interval during the following steps for reaction monitoring. In another flask, 10 mL of 15 mM $NaBH_4$ (5.72 mg) was prepared in ethanol. The $NaBH_4$ in EtOH solution (100 µL, 1 eq.) was added dropwise to the solution of **2**. DCM (50 µL) was added, and the solution was mixed. The reaction mixture was allowed to warm at room temperature and monitored for 2.0 hours.

S3.2.4. Reaction Monitoring Trends of $[Au_{24}(NHC)_{14}Cl_2H_3][BF_4]_3$ (5) synthesis

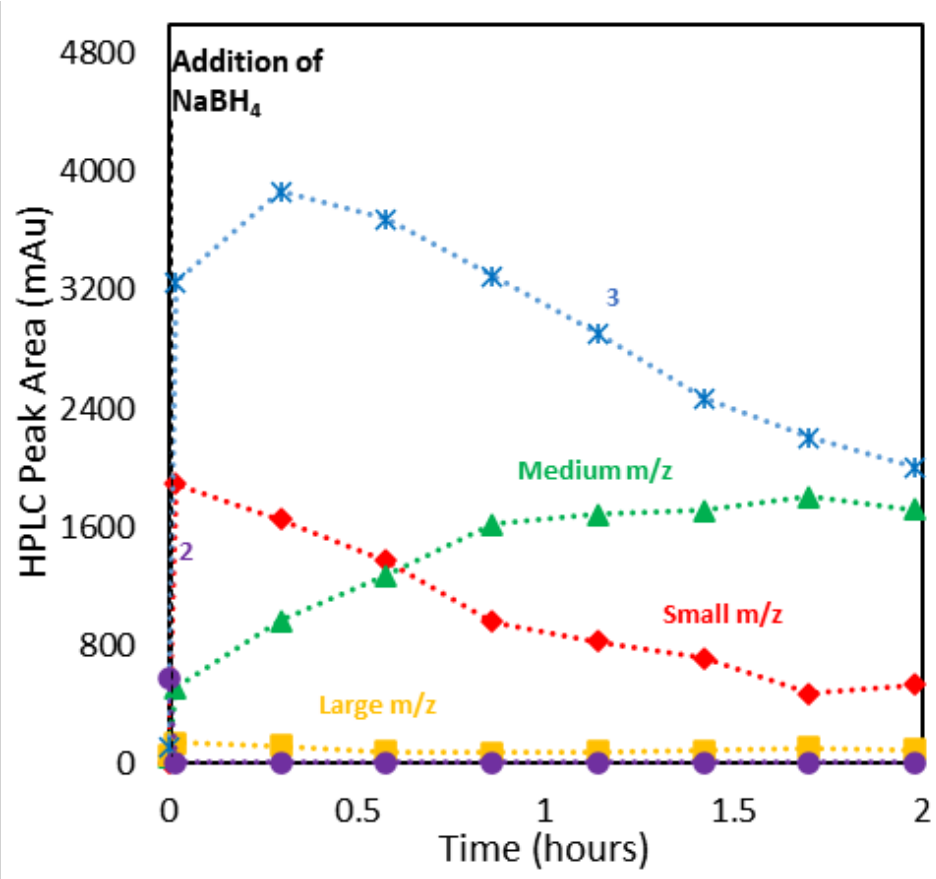

Figure S 3. HPLC monitoring of major products and regional analysis size regions in the synthesis of (**5**). Blue star (**3**), red diamond (small cluster region), green triangle (medium cluster region), yellow square (large cluster region). The first data point after the zero point was obtained 1 minute after addition of $NaBH_4$.

S4. MS signal found in regional analysis for Au_{13} (4) synthesis

S4.1. Small *m/z* region

In this section, we elucidate the process through which the ESI-MS data were extracted to monitor reaction trends (**Figure 3**). For the small mass-to-charge (*m/z*) region, we selected a retention time window of 6.5-8.5 minutes (**Figure 2**, highlighted in red), and the *m/z* scope for the extracted data was designated as 1000-3000 m/z. In the initial spectrum (**Figure S4**, only **1** dissolved in DCM), a prominent signal at *m/z* 1025 was evident. This substantial signal corresponds to the NHC-Au-Cl starting material **1** and the dimer $[NHC\text{-}Au]_2Cl^+$. This *m/z* 1025 signal was no longer observed following the addition of $NaBH_4$. Post $NaBH_4$ addition (refer to **Figure S5**), a series of MS signals emerged in the spectrum, with the principal ones being at *m/z* 1517.3, 1884.3, 1991.1, 2059.6, and 2590.0.

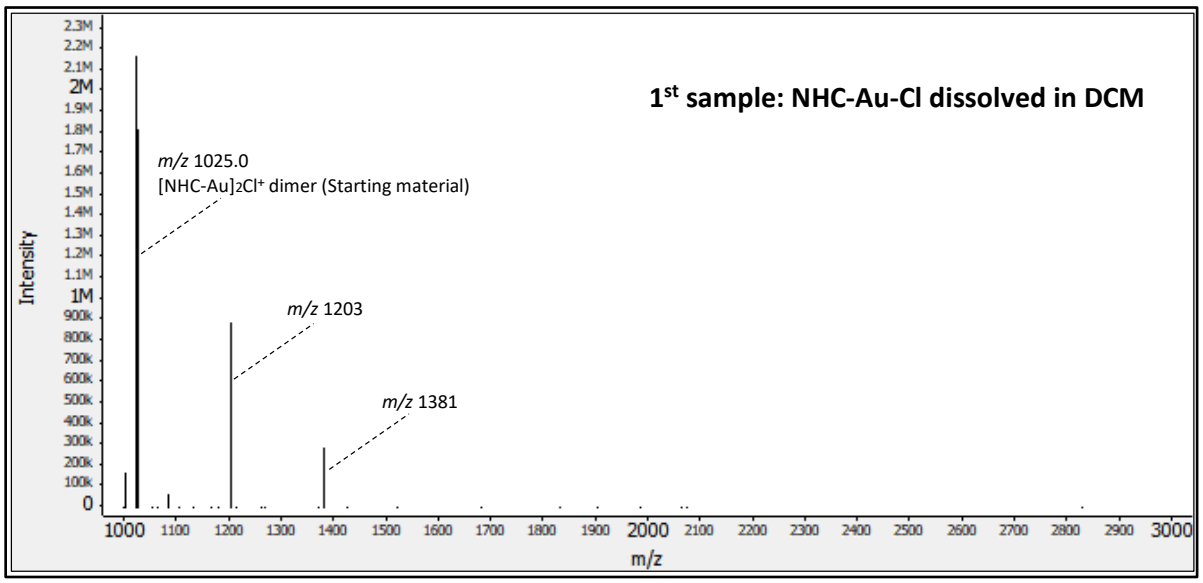

Figure S 4 Small *m/z* region mass spectrometry analysis for Au_{13} NC synthesis, selected *m/z* range: 1000-3000; selected retention time range: 6.5-8.5 minutes; reaction time point: 0 min

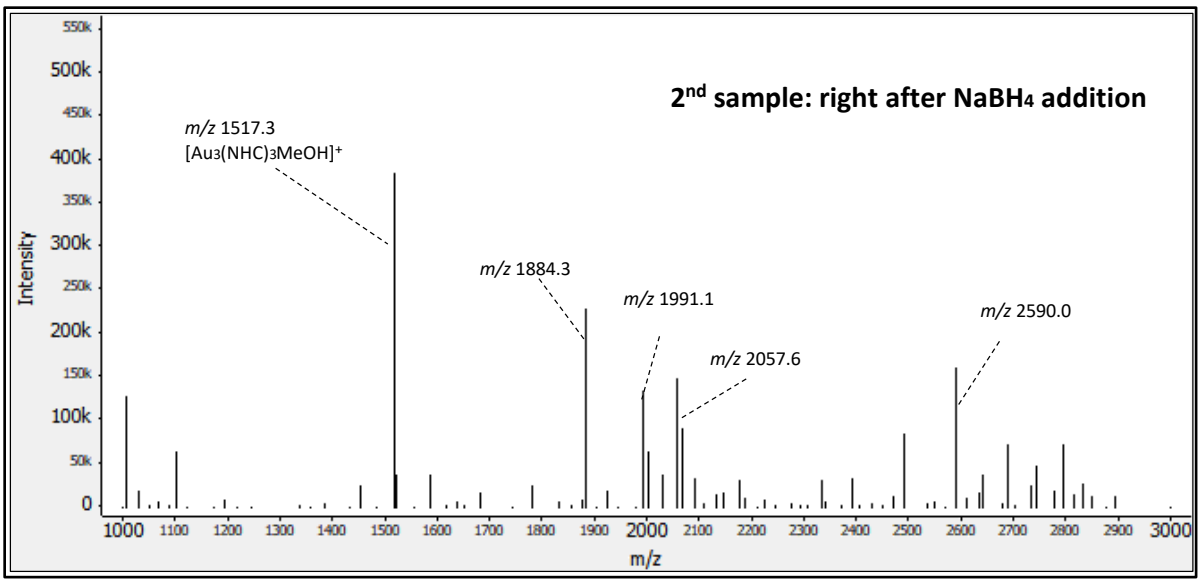

Figure S 5. Small *m/z* region mass spectrometry analysis for Au_{13} NC synthesis, selected *m/z* range: 1000-3000; selected retention time range: 6.5-8.5 minutes; reaction time point: 1 min

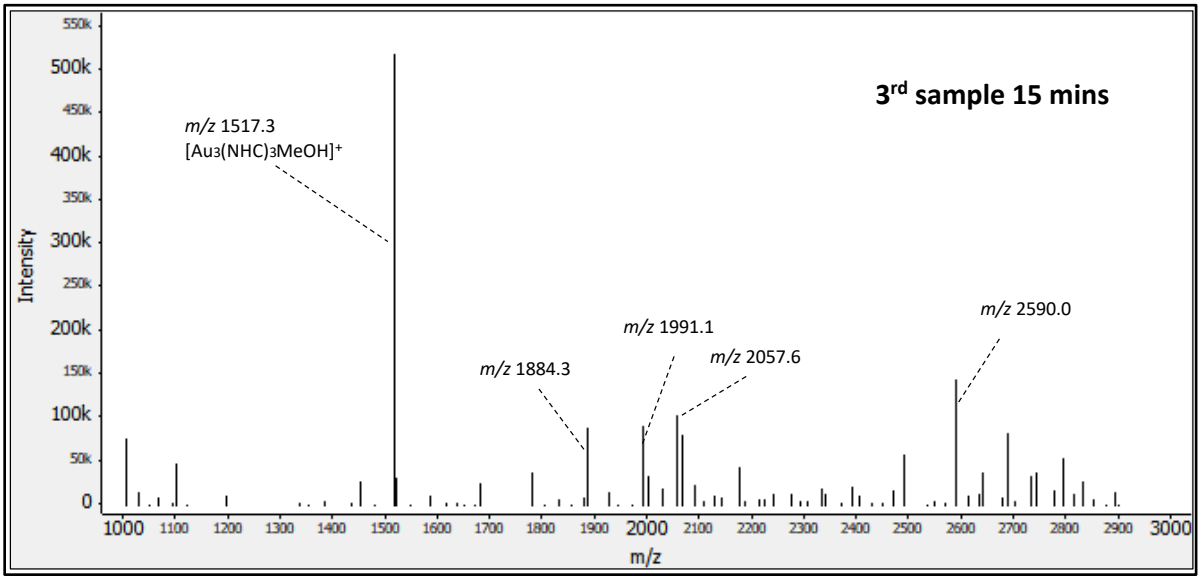

Figure S 6. Small *m/z* region mass spectrometry analysis for Au_{13} NC synthesis, selected *m/z* range: 1000-3000; selected retention time range: 6.5-8.5 minutes; reaction time point: 15 min

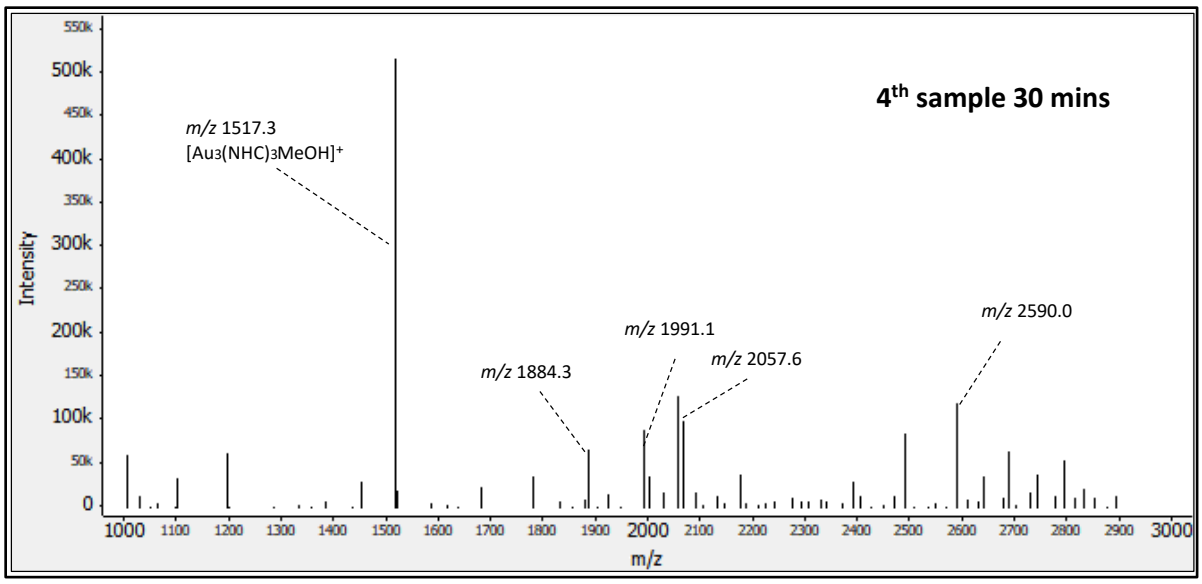

Figure S 7. Small *m/z* region mass spectrometry analysis for Au_{13} NC synthesis, selected *m/z* range: 1000-3000; selected retention time range: 6.5-8.5 minutes; reaction time point: 30 min

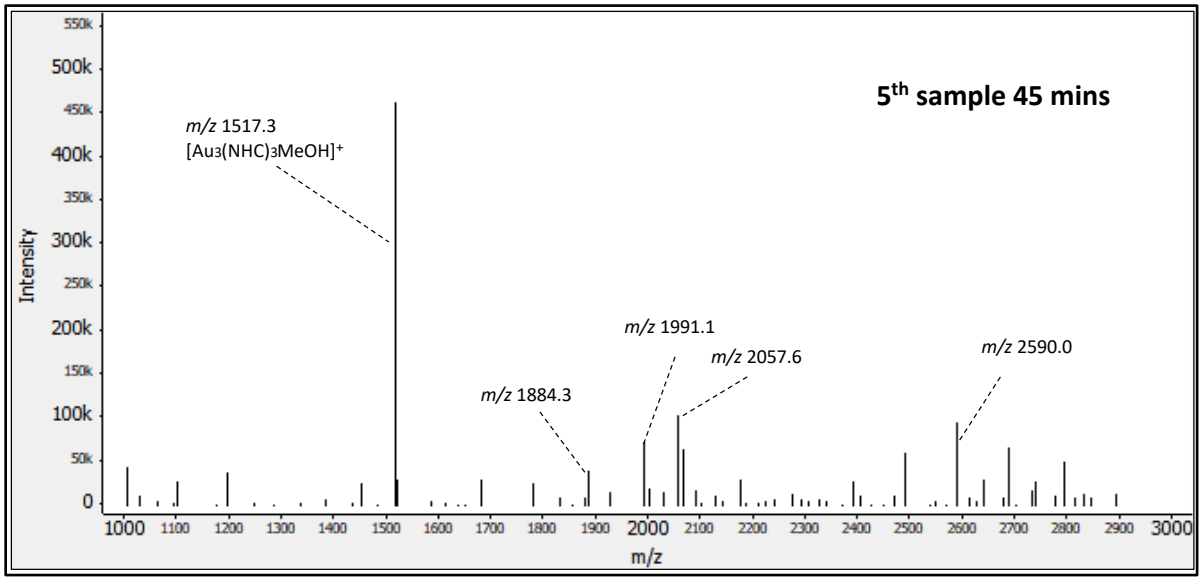

Figure S 8. Small *m/z* region mass spectrometry analysis for Au_{13} NC synthesis, selected *m/z* range: 1000-3000; selected retention time range: 6.5-8.5 minutes; reaction time point: 45 min

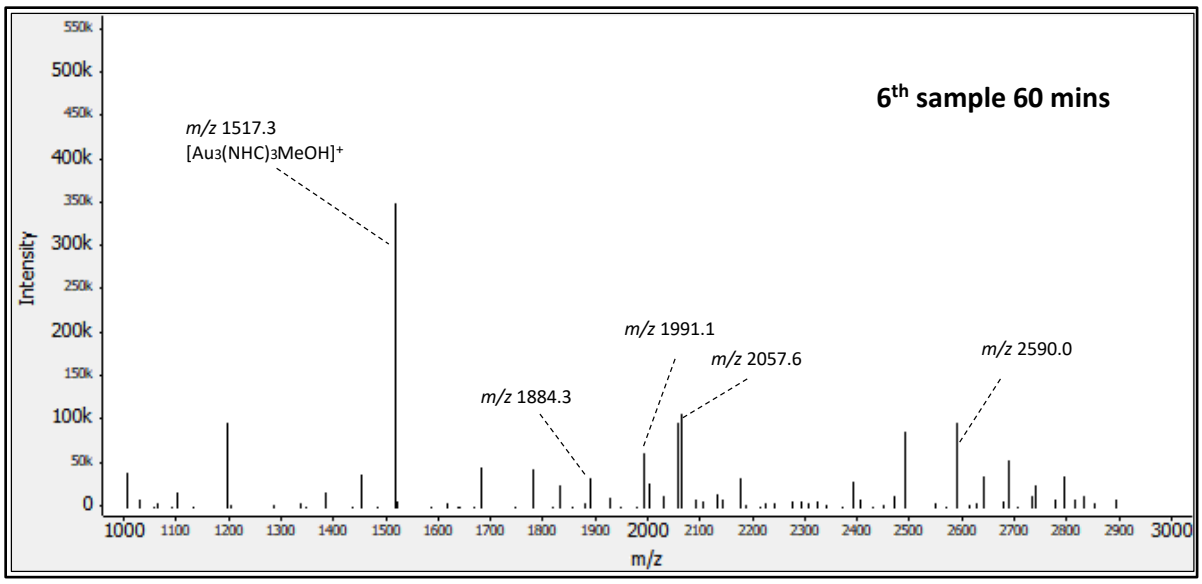

Figure S 9 Small *m/z* region mass spectrometry analysis for Au_{13} NC synthesis, selected *m/z* range: 1000-3000; selected retention time range: 6.5-8.5 minutes; reaction time point: 60 min

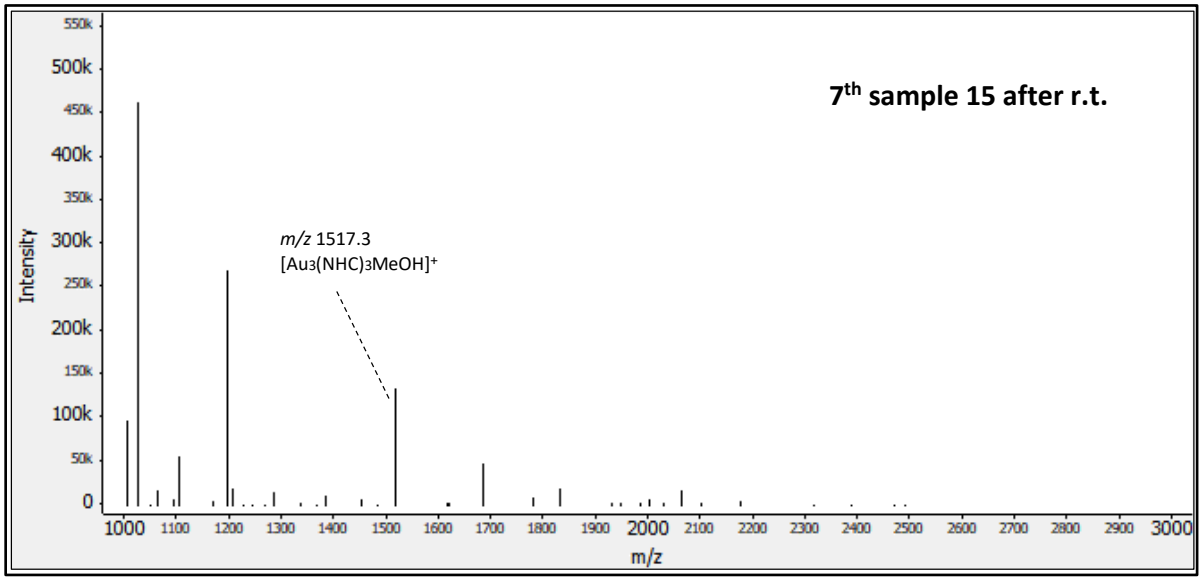

Figure S 10. Small *m/z* region mass spectrometry analysis for Au_{13} NC synthesis, selected *m/z* range: 1000-3000; selected retention time range: 6.5-8.5 minutes; reaction time point: 75 min

S4.2. Medium *m/z* region

In this segment, we explain how the ESI-MS data were extracted to monitor the reaction in the medium *m/z* region (retention time of 8.5-9.0 minutes) as shown in **Figure 3** (this range is highlighted in green in **Figure 2**). The *m/z* scope set for these extracted data ranged from 1000 to 3000 m/z. Following the addition of $NaBH_4$ (as per **Figure S11**), a series of MS signals surfaced in the spectrum, including those at *m/z* 2675.7, corresponding to $[Au_{13}(NHC)_9Cl_3]^{2+}$ (**4**), and *m/z* 2774.7, corresponding to $[Au_{14}(NHC)_9Cl_3]^{2+}$. The reciprocal interplay between these two species is readily discernible in the MS spectra: as the reaction proceeded, species **3** and **4** were initially formed with a relatively lower MS intensity than Au_{14}. However, the intensity of Au_{14} began to decrease as that of species **4** increased. After eight samples, the relative MS intensity reversed. It's noteworthy that, unlike the analysis for the small *m/z* region, the MS signals within the 1000-2500 *m/z* range remained low.

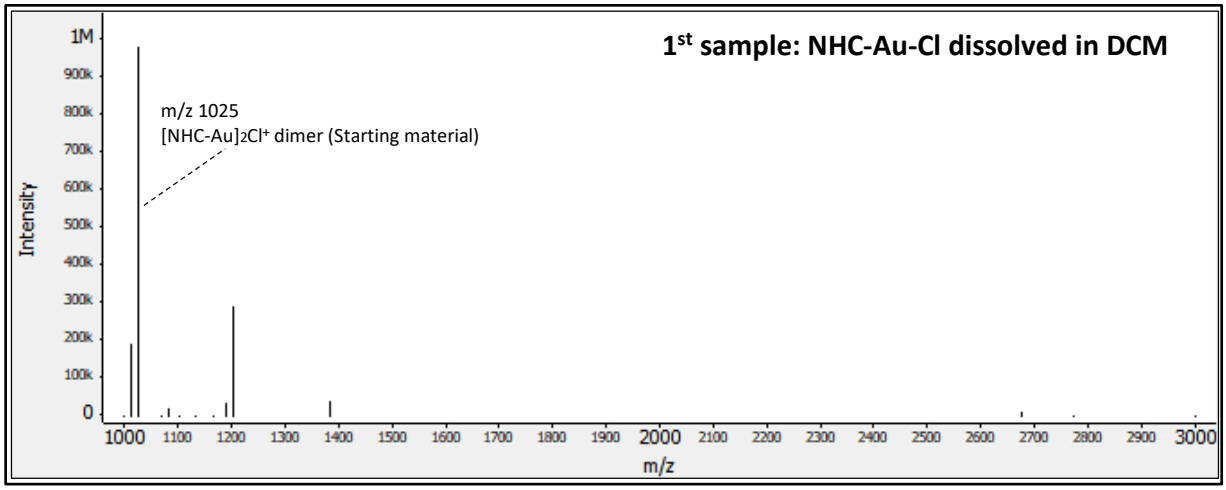

Figure S 11. Medium *m/z* region mass spectrometry analysis for Au_{13} NC synthesis, selected *m/z* range: 1000-3000; selected retention time range: 8.5-9.0 minutes; reaction time point: 0 min

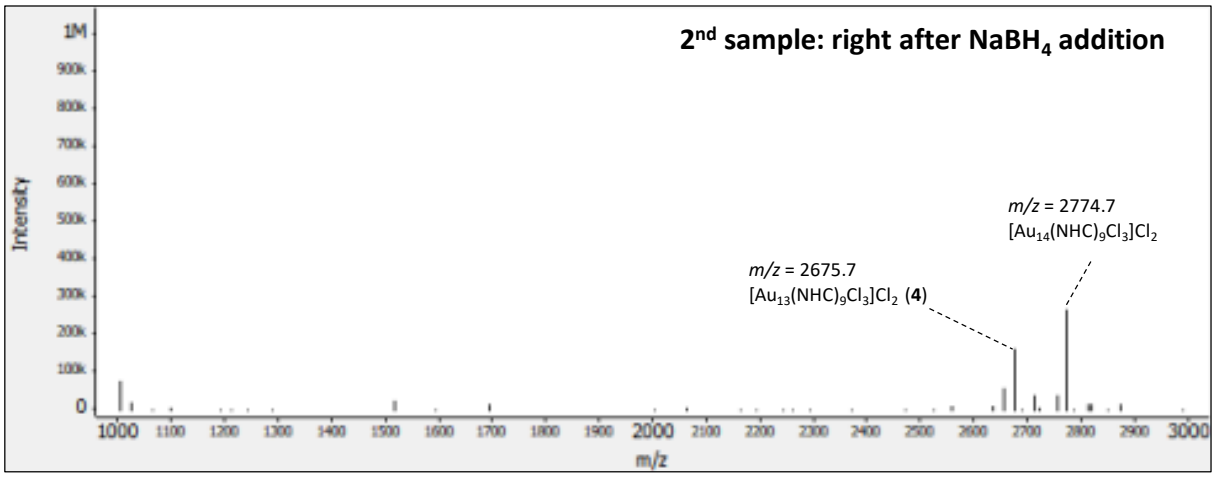

Figure S 12. Medium *m/z* region mass spectrometry analysis for Au_{13} NC synthesis, selected *m/z* range: 1000-3000; selected retention time range: 8.5-9.0 minutes; reaction time point: 1 min

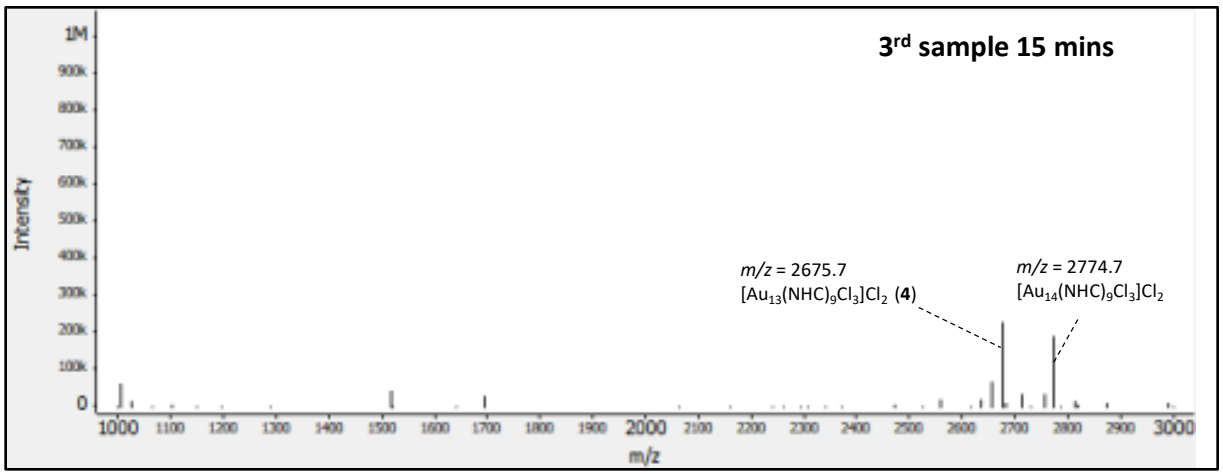

Figure S 13. Medium *m/z* region mass spectrometry analysis for Au_{13} NC synthesis, selected *m/z* range: 1000-3000; selected retention time range: 8.5-9.0 minutes; reaction time point: 15 min

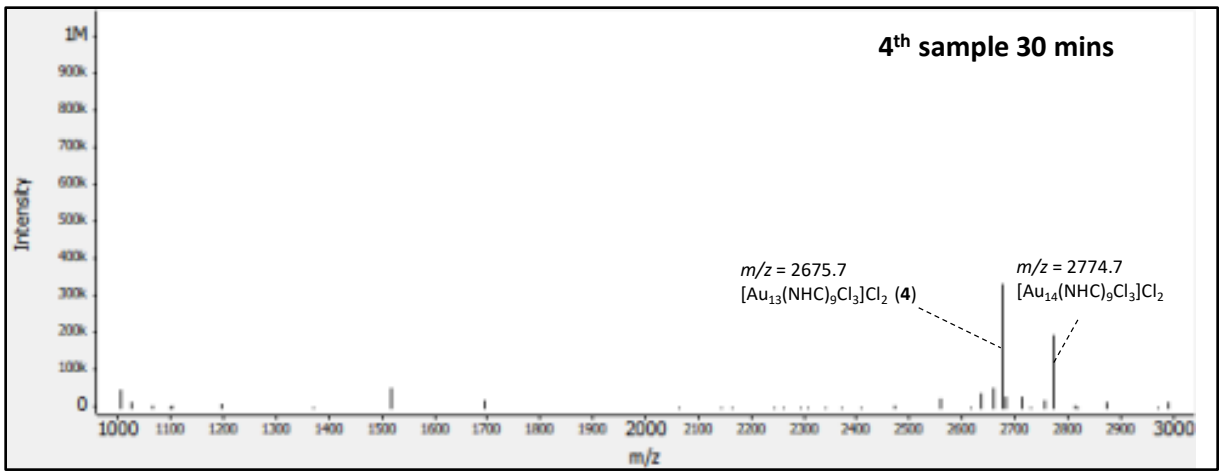

Figure S 14. Medium *m/z* region mass spectrometry analysis for Au_{13} NC synthesis, selected *m/z* range: 1000-3000; selected retention time range: 8.5-9.0 minutes; reaction time point: 30 min

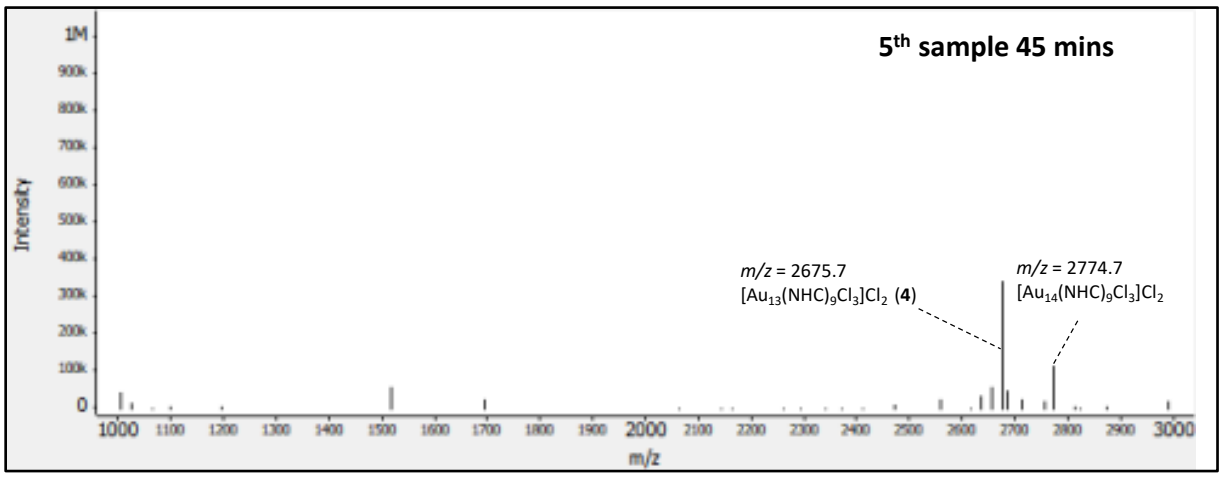

Figure S 15. Medium *m/z* region mass spectrometry analysis for Au_{13} NC synthesis, selected *m/z* range: 1000-3000; selected retention time range: 8.5-9.0 minutes; reaction time point: 45 min

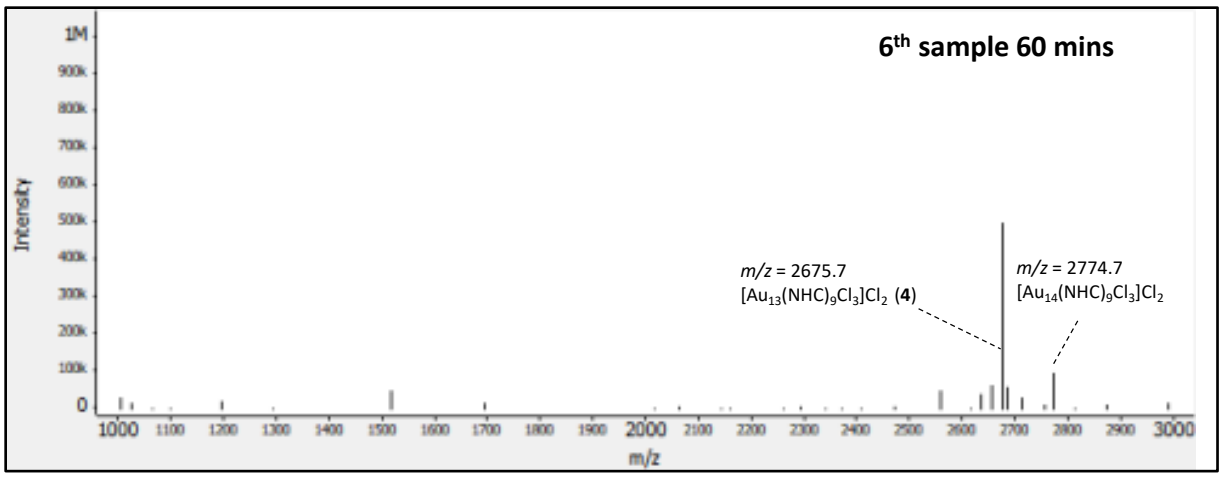

Figure S 16. Medium *m/z* region mass spectrometry analysis for Au_{13} NC synthesis, selected *m/z* range: 1000-3000; selected retention time range: 8.5-9.0 minutes; reaction time point: 60 min

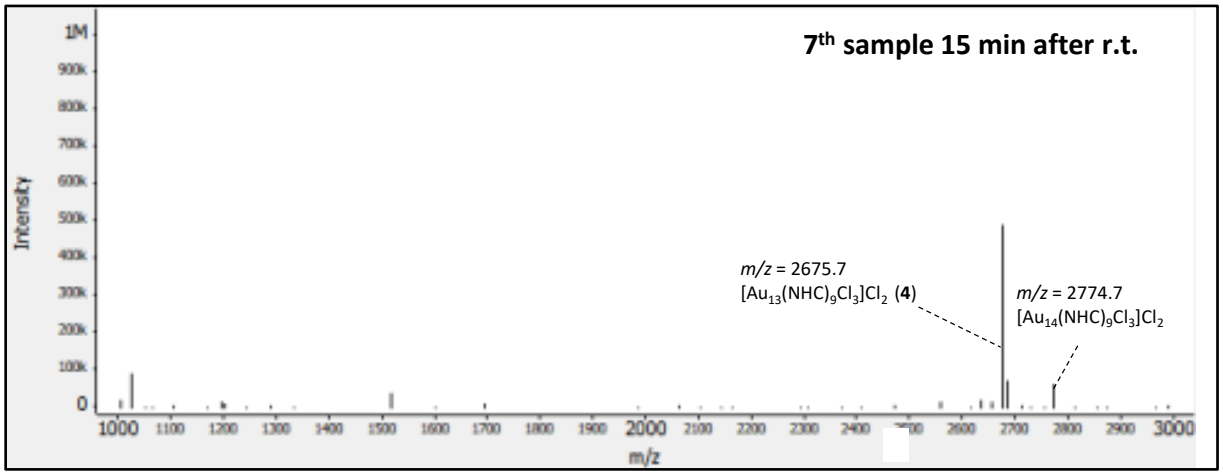

Figure S 17. Medium *m/z* region mass spectrometry analysis for Au_{13} NC synthesis, selected *m/z* range: 1000-3000; selected retention time range: 8.5-9.0 minutes; reaction time point: 75 min

S5. MS signal found in regional analysis for Au_{24} (5) synthesis

S5.1. Small *m/z* region

In this segment, we explain how the ESI-MS data were extracted to monitor the reaction in the medium *m/z* region (retention time of 8.5-9.0 minutes) as shown in **Figure 8** (this range is highlighted in green in **Figure 2**). The *m/z* scope set for these extracted data ranged from 1000 to 3000 *m/z*. Following the addition of $NaBH_4$ (as per **Figure S18**, only **2** dissolved in toluene), a series of MS signals surfaced in the spectrum, including those at *m/z* 2675.7, corresponding to $[Au_{13}(NHC)_9Cl_3]^{2+}$ (**4**), and *m/z* 2774.7, corresponding to $[Au_{14}(NHC)_9Cl_3]^{2+}$. The reciprocal interplay between these two species is readily discernible in the MS spectra: as the reaction proceeded, species **3** and **4** were initially formed with a relatively lower MS intensity than Au_{14}. However, the intensity of Au_{14} began to decrease as that of species **4** increased. After eight samples, the relative MS intensity reversed. It's noteworthy that, unlike the analysis for the small *m/z* region, the MS signals within the 1000-2500 *m/z* range remained low.

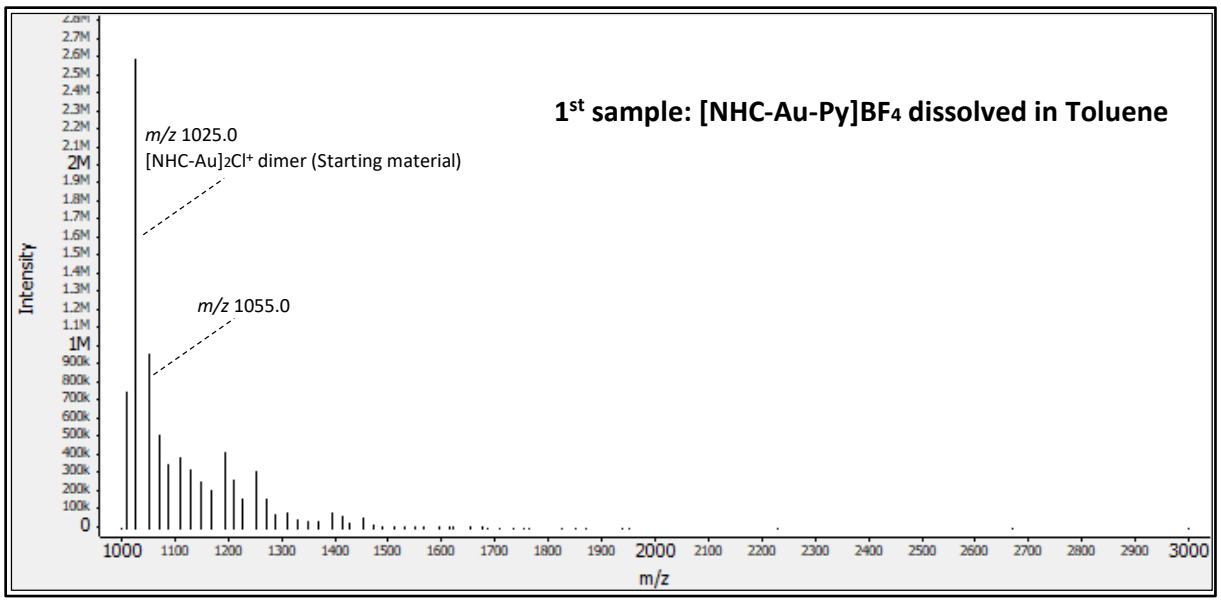

Figure S 18. Small *m/z* region mass spectrometry analysis for Au_{24} NC synthesis, selected *m/z* range: 1000-3000; selected retention time range: 6.5-8.5 minutes; reaction time point: 0 min

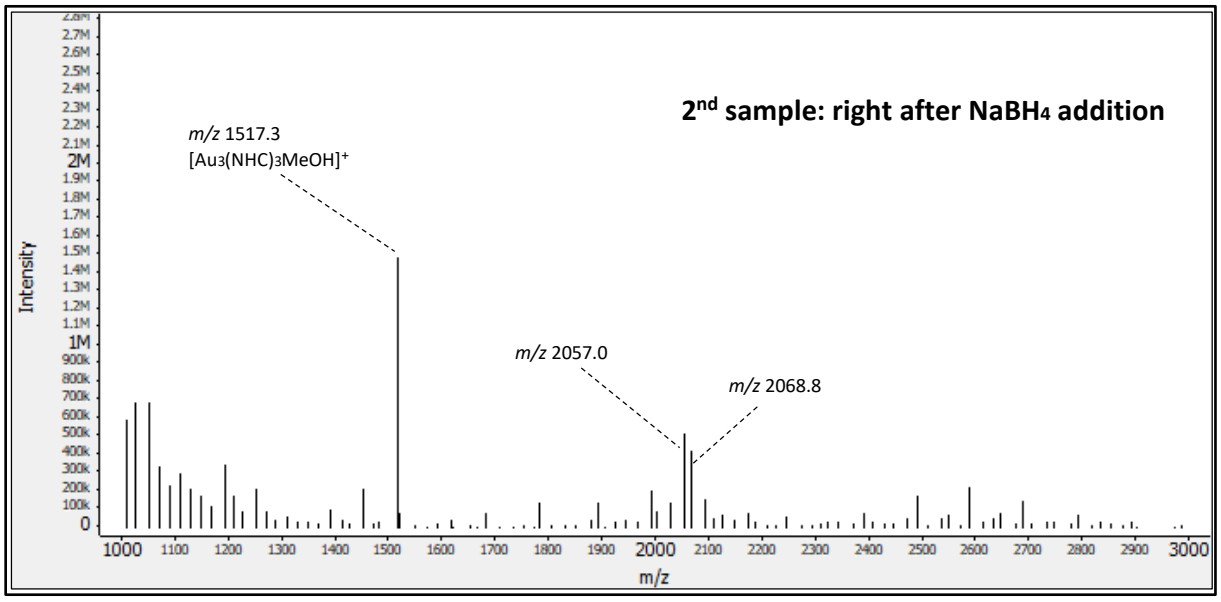

Figure S 19. Small *m/z* region mass spectrometry analysis for Au_{24} NC synthesis, selected *m/z* range: 1000-3000; selected retention time range: 6.5-8.5 minutes; reaction time point: 1 min

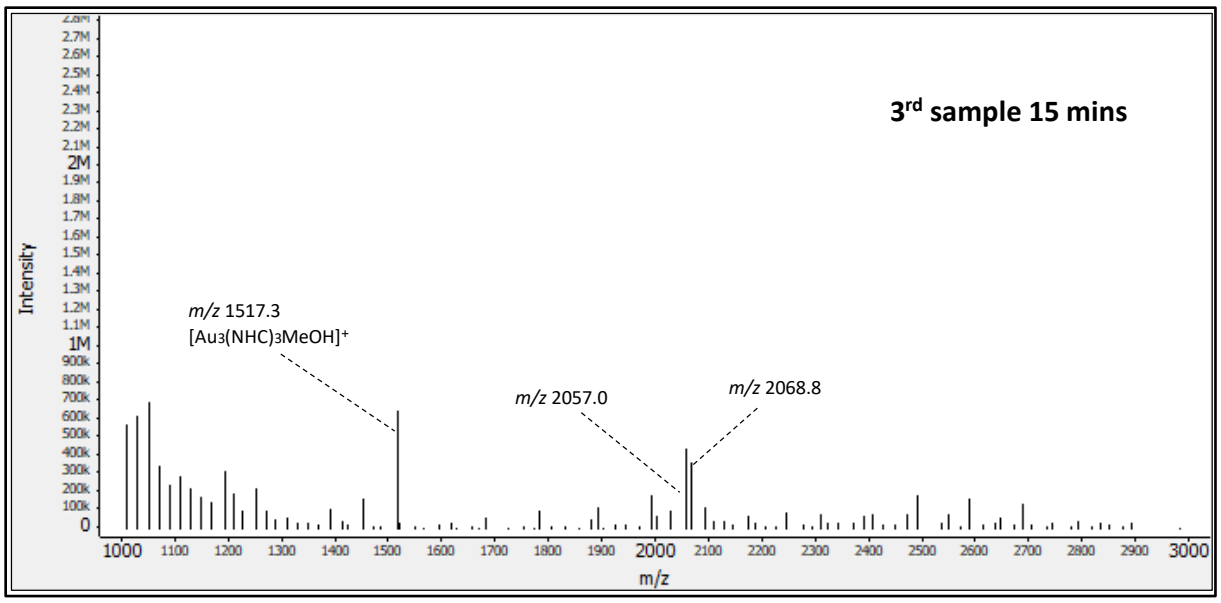

Figure S 20. Small *m/z* region mass spectrometry analysis for Au_{24} NC synthesis, selected *m/z* range: 1000-3000; selected retention time range: 6.5-8.5 minutes; reaction time point: 15 min

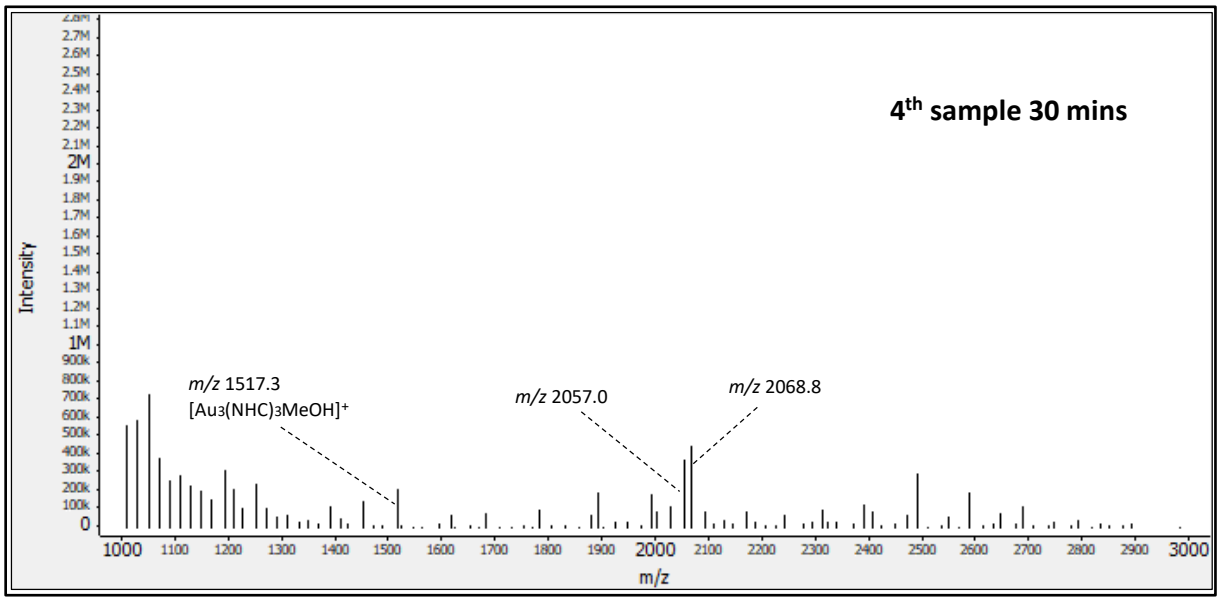

Figure S 21. Small *m/z* region mass spectrometry analysis for Au_{24} NC synthesis, selected *m/z* range: 1000-3000; selected retention time range: 6.5-8.5 minutes; reaction time point: 30 min

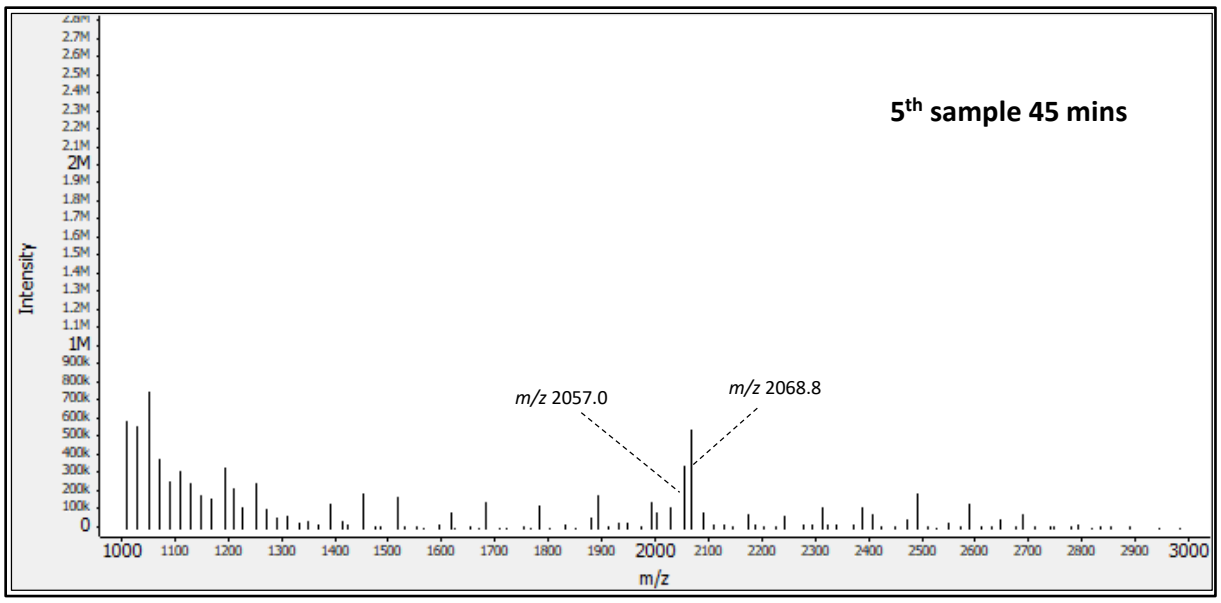

Figure S 22. Small *m/z* region mass spectrometry analysis for Au_{24} NC synthesis, selected *m/z* range: 1000-3000; selected retention time range: 6.5-8.5 minutes; reaction time point: 45 min

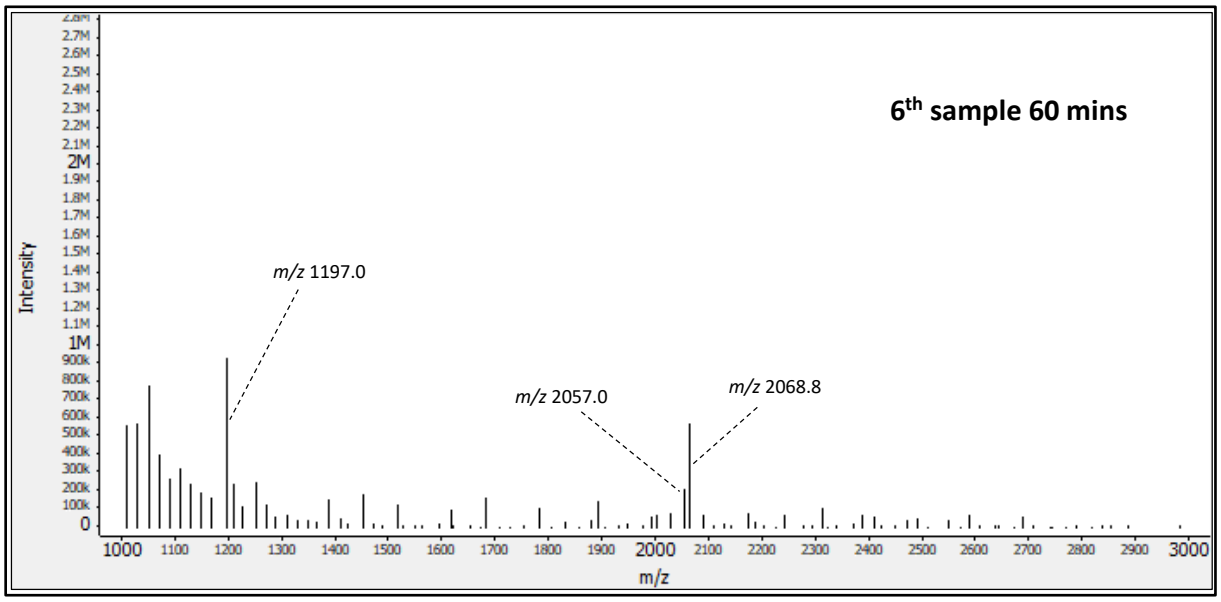

Figure S 23. Small *m/z* region mass spectrometry analysis for Au_{24} NC synthesis, selected *m/z* range: 1000-3000; selected retention time range: 6.5-8.5 minutes; reaction time point: 60 min

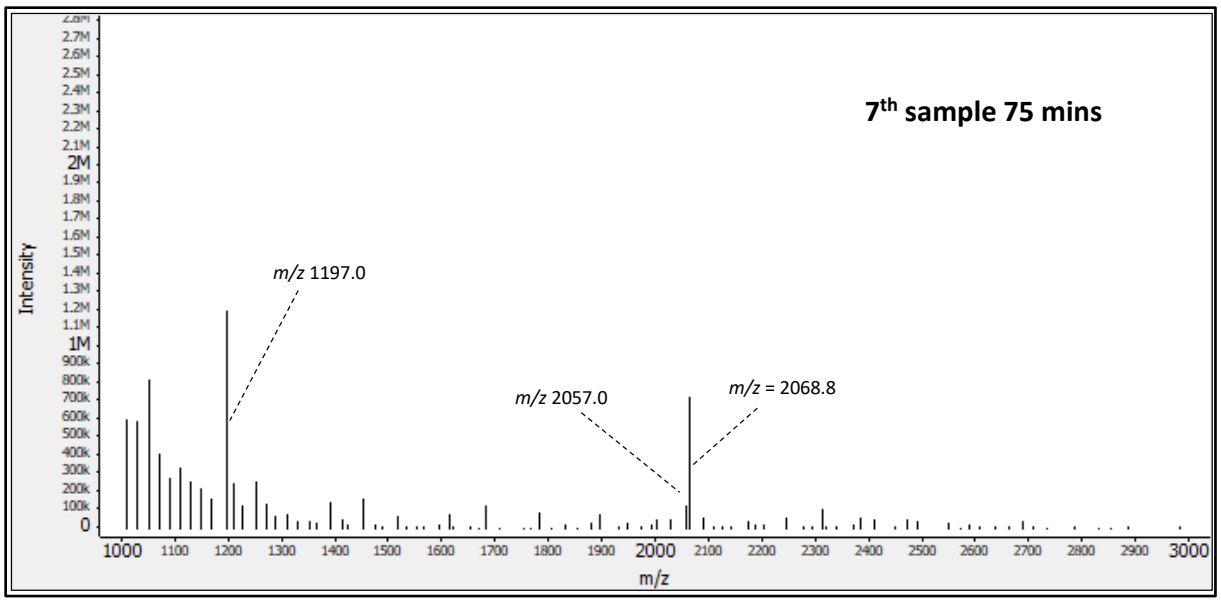

Figure S 24. Small *m/z* region mass spectrometry analysis for Au_{24} NC synthesis, selected *m/z* range: 1000-3000; selected retention time range: 6.5-8.5 minutes; reaction time point: 75 min

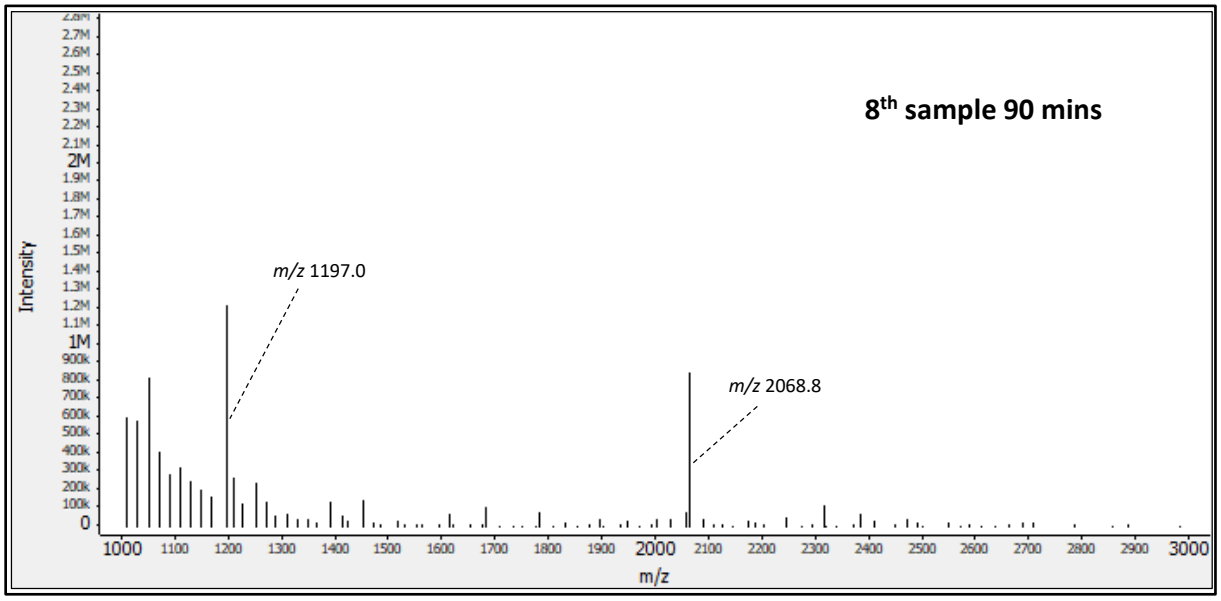

Figure S 25. Small *m/z* region mass spectrometry analysis for Au_{24} NC synthesis, selected *m/z* range: 1000-3000; selected retention time range: 6.5-8.5 minutes; reaction time point: 90 min

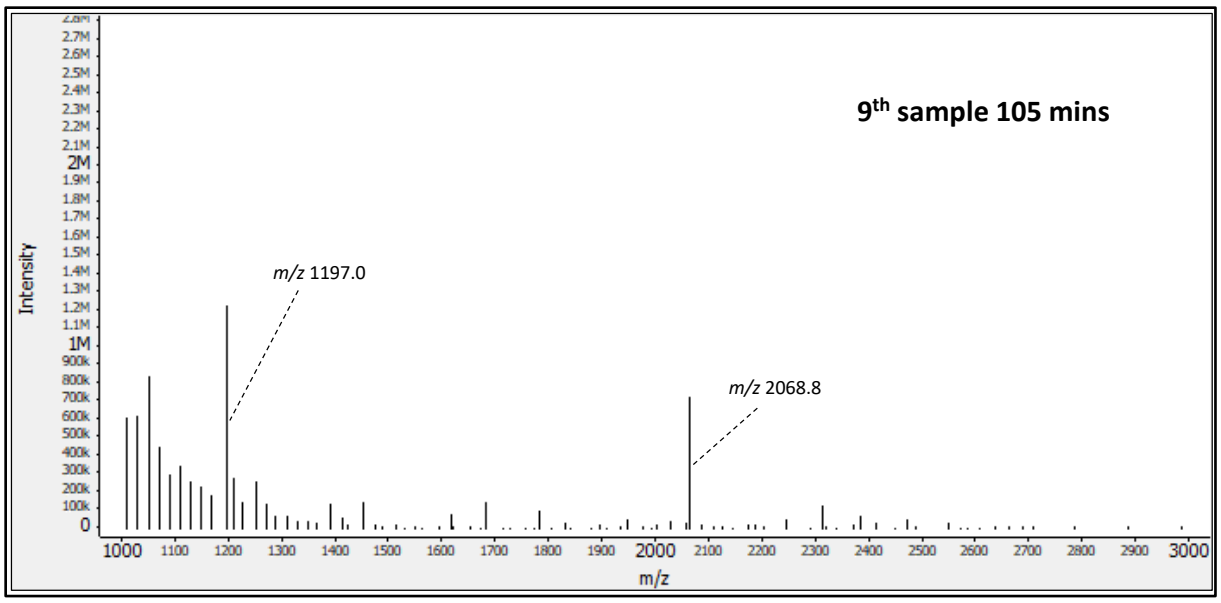

Figure S 26. Small *m/z* region mass spectrometry analysis for Au_{24} NC synthesis, selected *m/z* range: 1000-3000; selected retention time range: 6.5-8.5 minutes; reaction time point: 105 min

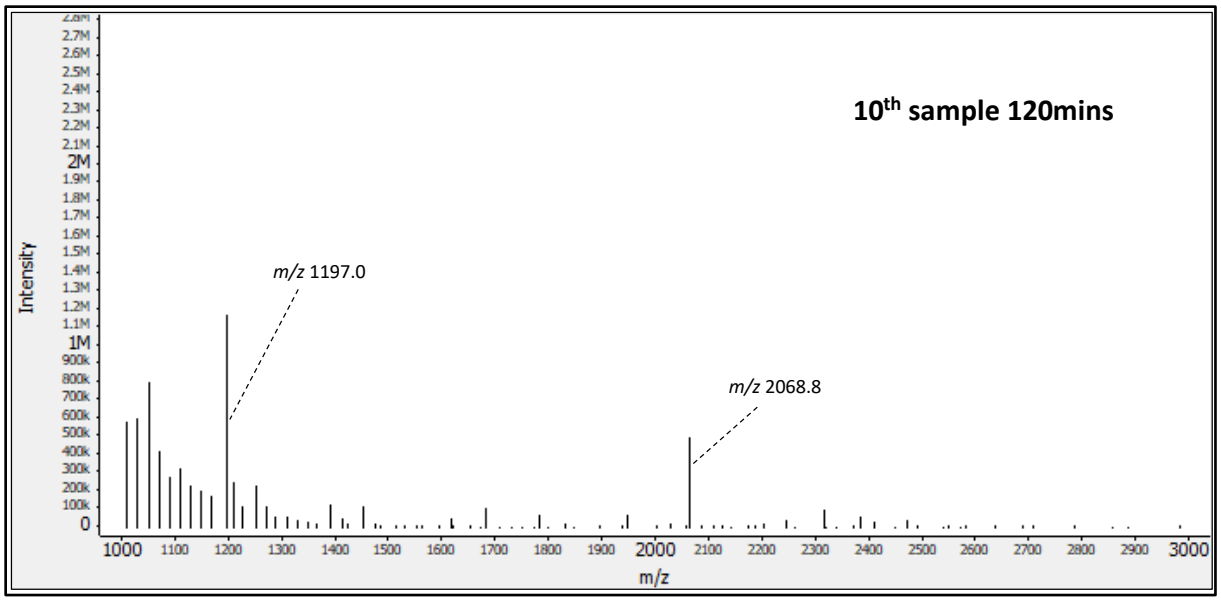

Figure S 27. Small *m/z* region mass spectrometry analysis for Au_{24} NC synthesis, selected *m/z* range: 1000-3000; selected retention time range: 6.5-8.5 minutes; reaction time point: 120 min

S5.2. Medium *m/z* region

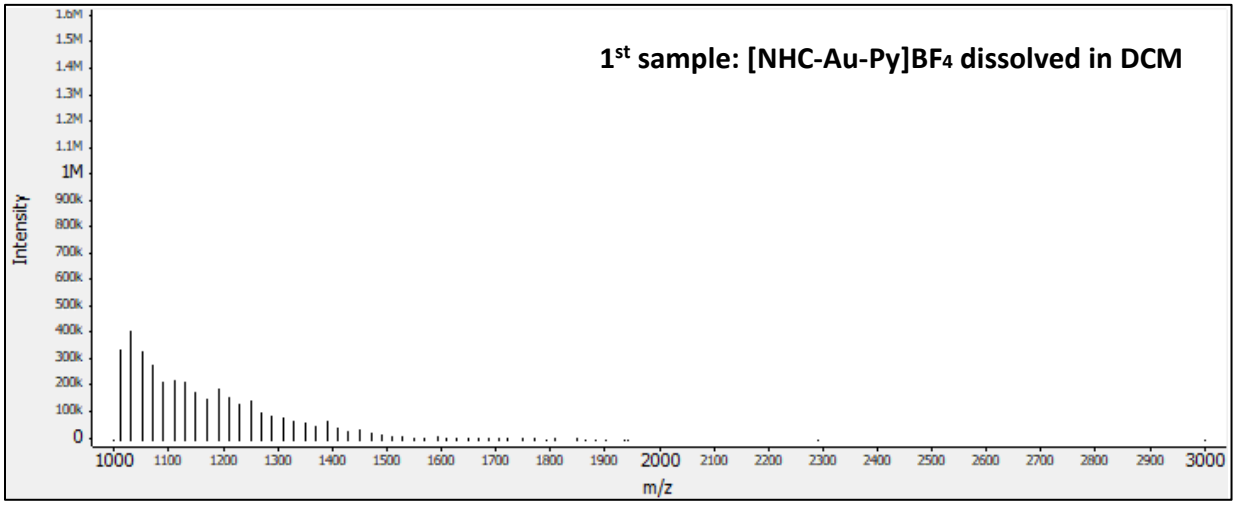

Figure S 28. Medium *m/z* region mass spectrometry analysis for Au_{24} NC synthesis, selected *m/z* range: 1000-3000; selected retention time range: 8.5-9.0 minutes; reaction time point: 0 min

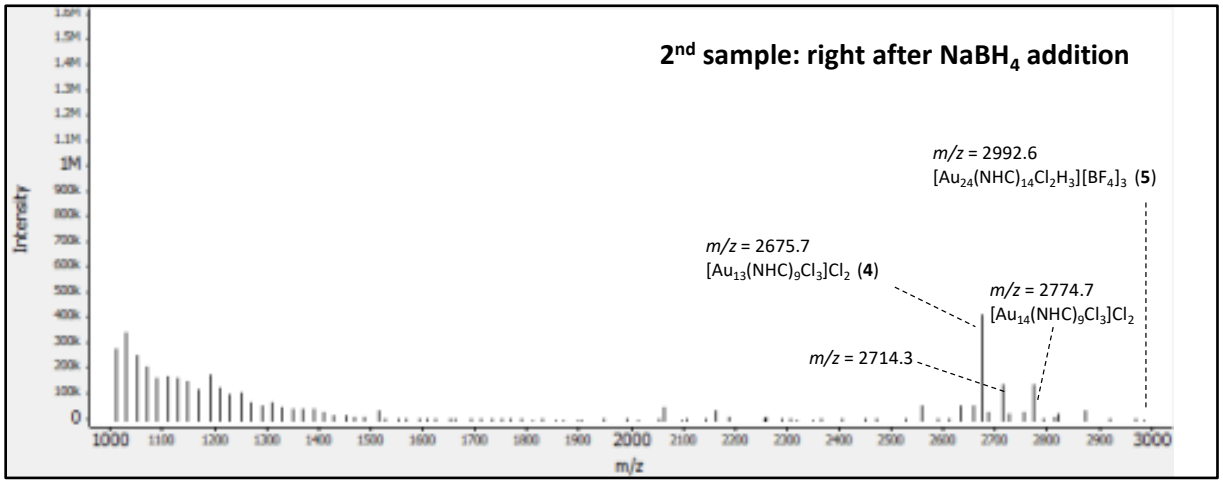

Figure S 29. Medium *m/z* region mass spectrometry analysis for Au_{24} NC synthesis, selected *m/z* range: 1000-3000; selected retention time range: 8.5-9.0 minutes; reaction time point: 1 min

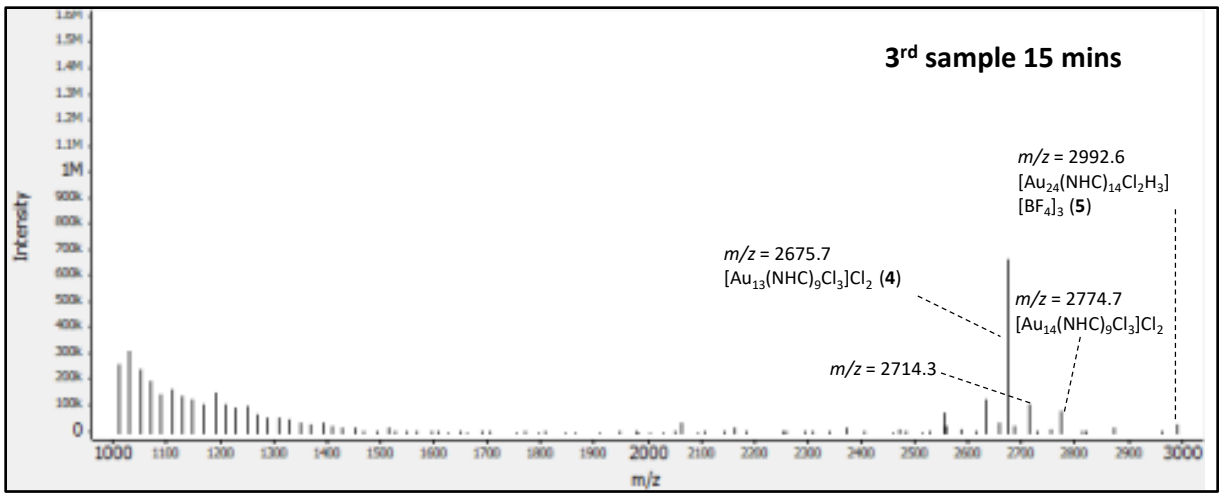

Figure S 30. Medium *m/z* region mass spectrometry analysis for Au_{24} NC synthesis, selected *m/z* range: 1000-3000; selected retention time range: 8.5-9.0 minutes; reaction time point: 15 min

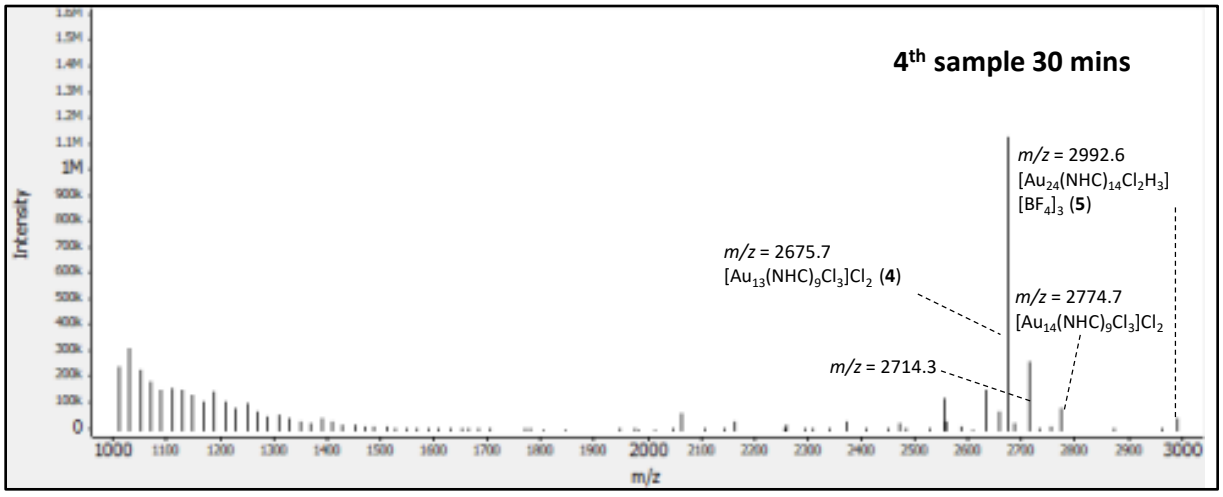

Figure S 31. Medium *m/z* region mass spectrometry analysis for Au_{24} NC synthesis, selected *m/z* range: 1000-3000; selected retention time range: 8.5-9.0 minutes; reaction time point: 30 min

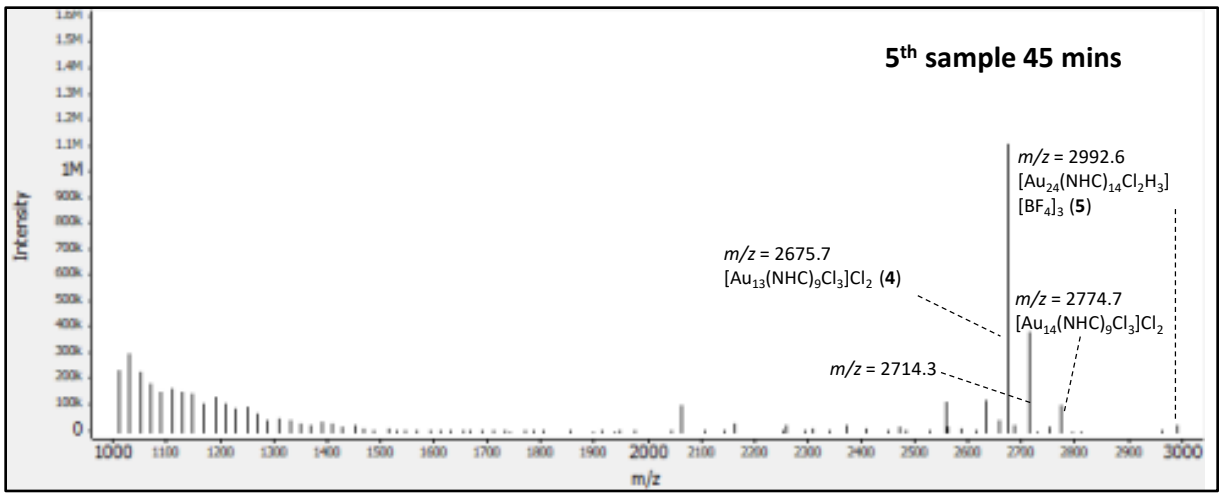

Figure S 32. Medium *m/z* region mass spectrometry analysis for Au_{24} NC synthesis, selected *m/z* range: 1000-3000; selected retention time range: 8.5-9.0 minutes; reaction time point: 45 min

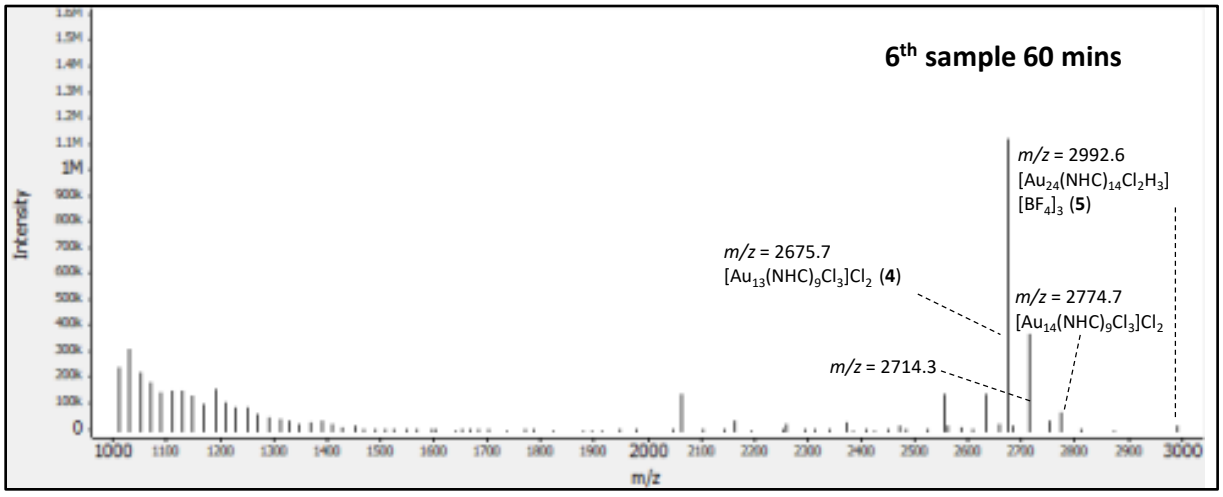

Figure S 33. Medium *m/z* region mass spectrometry analysis for Au_{24} NC synthesis, selected *m/z* range: 1000-3000; selected retention time range: 8.5-9.0 minutes; reaction time point: 60 min

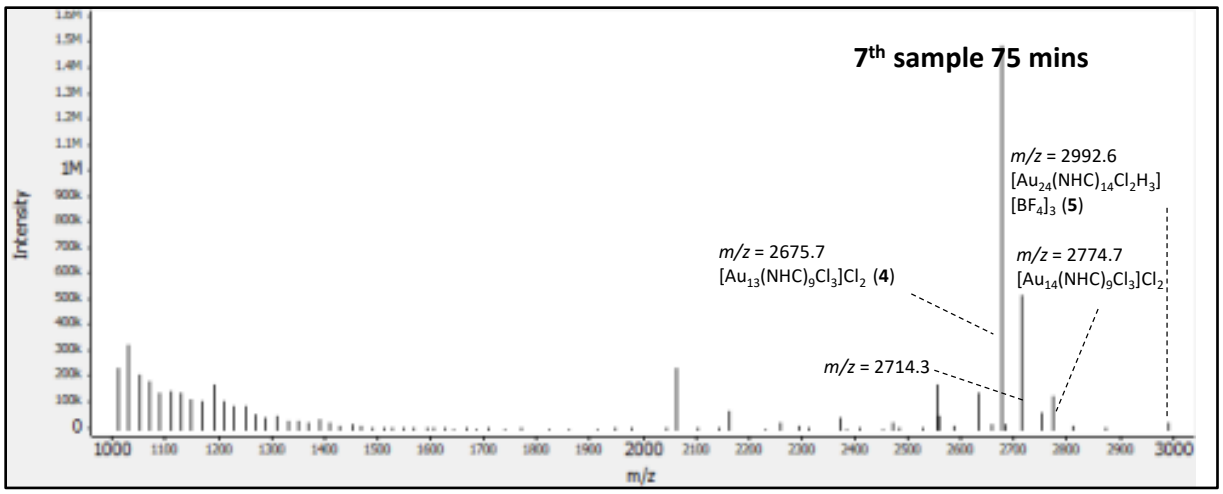

Figure S 34. Medium *m/z* region mass spectrometry analysis for Au_{24} NC synthesis, selected *m/z* range: 1000-3000; selected retention time range: 8.5-9.0 minutes; reaction time point: 75 min

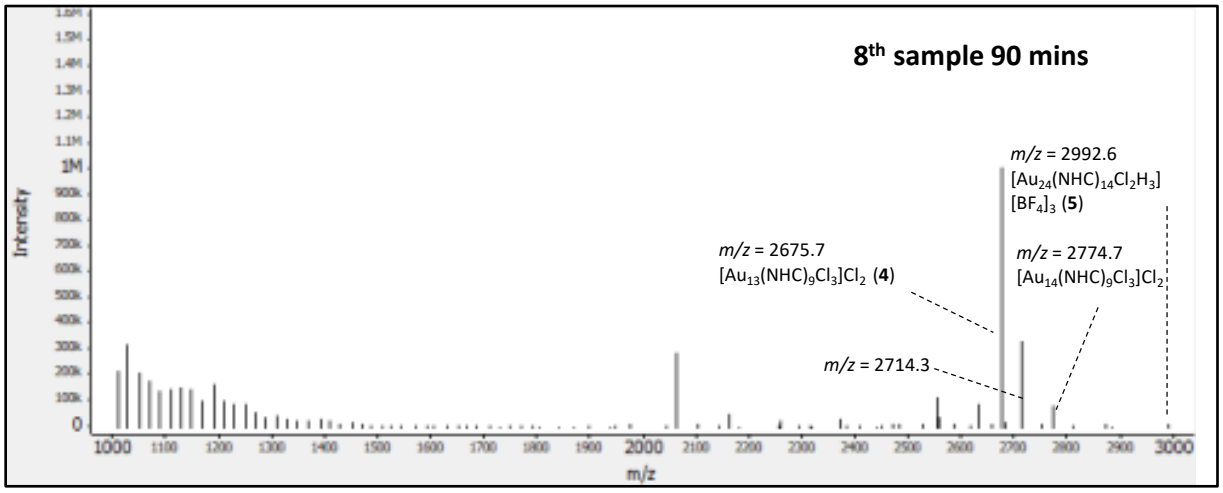

Figure S 35. Medium *m/z* region mass spectrometry analysis for Au_{24} NC synthesis, selected *m/z* range: 1000-3000; selected retention time range: 8.5-9.0 minutes; reaction time point: 90 min

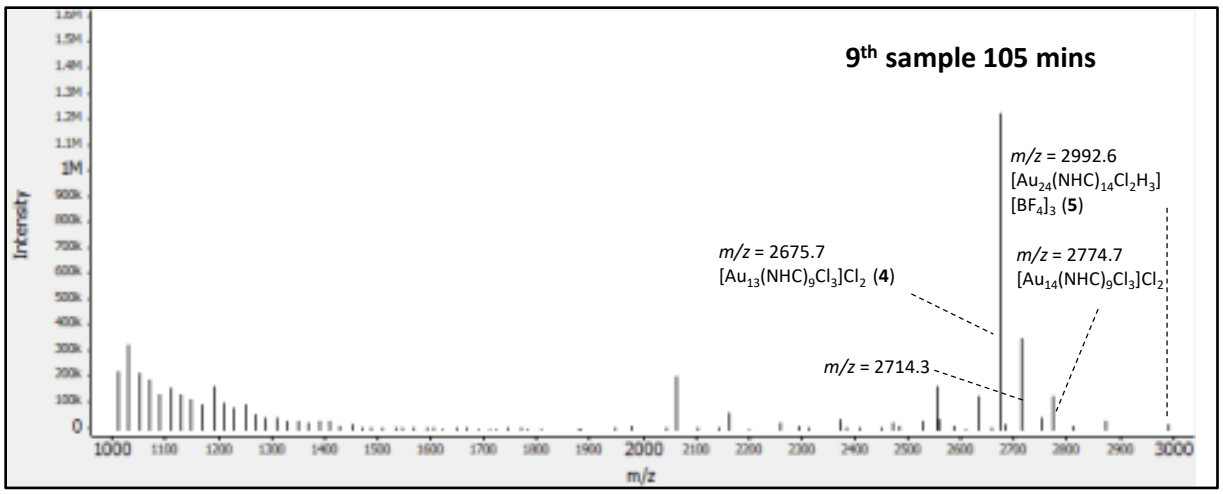

Figure S 36. Medium *m/z* region mass spectrometry analysis for Au_{24} NC synthesis, selected *m/z* range: 1000-3000; selected retention time range: 8.5-9.0 minutes; reaction time point: 105 min

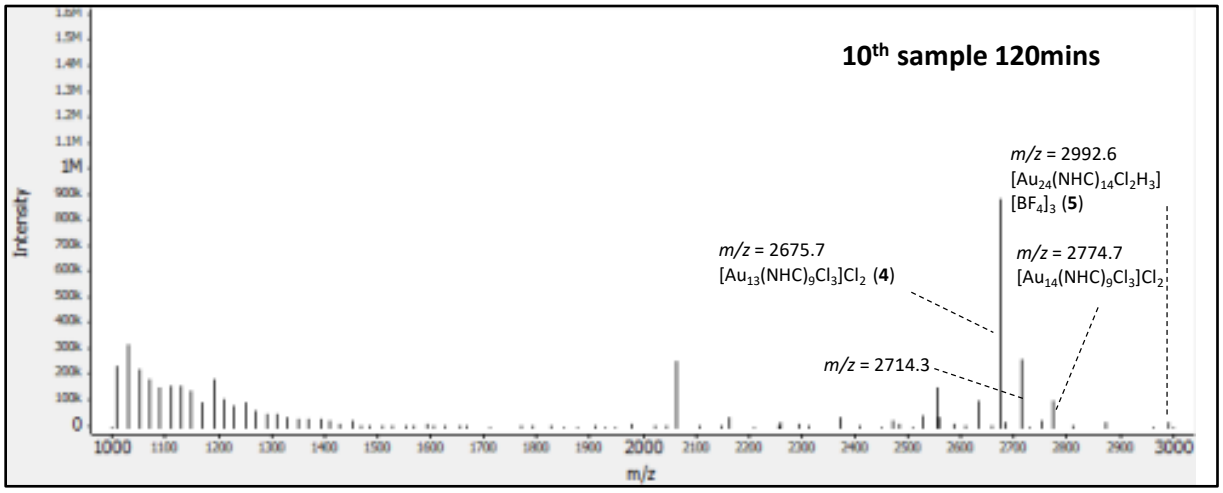

Figure S 37. Medium *m/z* region mass spectrometry analysis for Au_{24} NC synthesis, selected *m/z* range: 1000-3000; selected retention time range: 8.5-9.0 minutes; reaction time point: 120 min

S6. HPLC spectra comparison between synthesis of 4 and 5

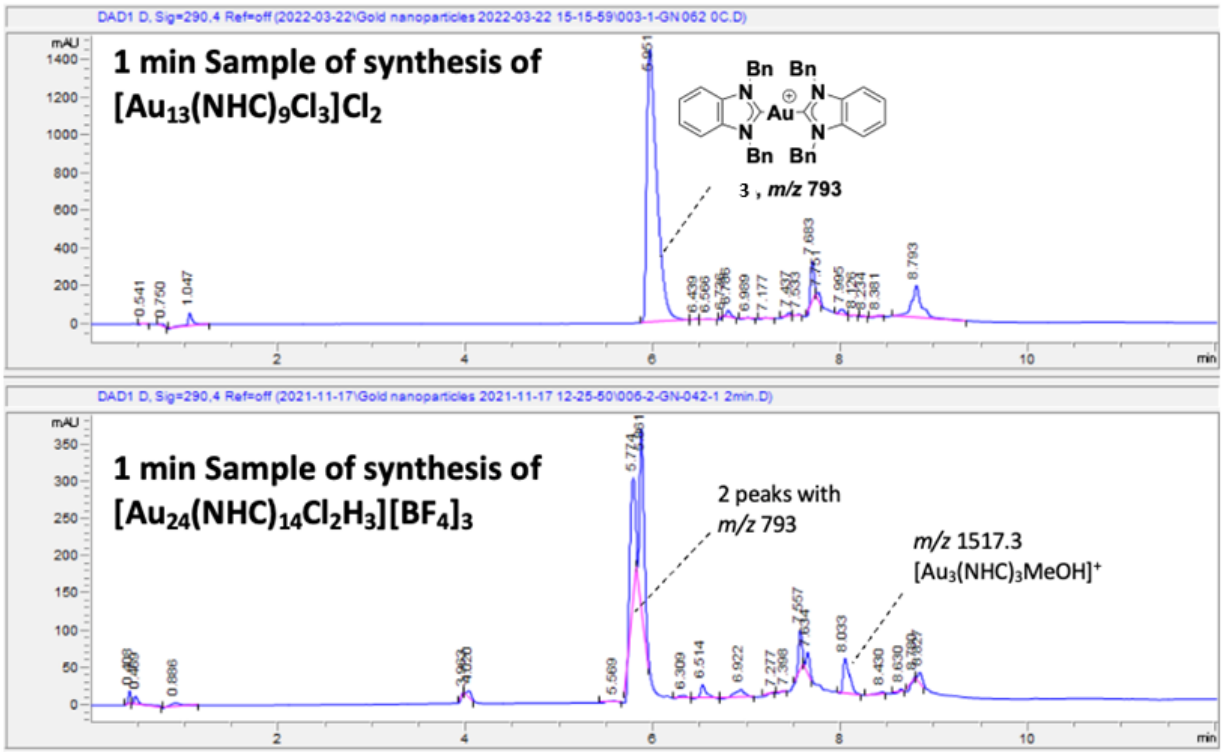

Figure S 38. HPLC chromatogram comparison between the synthesis of 4 and 5. Reaction samples at 1 minute point from each reaction were compared using 290 nm wavelength.

The HPLC spectrum of compound **5** synthesis demonstrated the presence of two peaks with a mass-to-charge ratio (*m/z*) of 793. This *m/z* coincides with that of the bis-NHC complex byproduct **3**. Given that [NHC-Au-Py]BF_4 (**2**) was utilized as the starting material, these two peaks could signify the presence of [NHC-Au-NHC]$^+$ coordinated with two distinct counter ions (BF_4^- and Cl^-). Although they possess identical *m/z* values, these compounds elute differently, likely due to their different ionic compositions. Additionally, the HPLC spectrum of compound **5** synthesis exhibited a significant amount of $[Au_3(NHC)_3MeOH]^+$, indicating the occurrence of this complex during the reaction process. This observation can provide important insights into the reaction mechanism and potential intermediates.

S7. Slow dose experiments for yield comparison

The sequential dose experiment, as depicted in **Figure 6** and **Figure 7**, suggested that this method could suppress the formation of clusters in the large region. However, the peak area in the medium region did not significantly increase compared to the original one-shot dose experiment shown in **Figure 3**. This discrepancy might be attributed to the absence of an internal standard, which could have led to sampling errors and solvent evaporation. Therefore, to refine our understanding, we designed experiments with an internal standard and calibration, as demonstrated in section **S2.5**:

- Experiment 1 entailed dosing 0.2 equivalents of a $NaBH_4$ solution (100 mM) each time, culminating in 5 additions in total, which made up 1.0 equivalent of the reducing reagent.
- Experiment 2 involved dosing 0.1 equivalents of a $NaBH_4$ solution (100 mM) each time, culminating in 10 additions in total, which also amounted to 1.0 equivalent of the reducing reagent.

While the total amount of $NaBH_4$ used by the end of both experiments was the same, the rate and timing of the additions varied. Following each $NaBH_4$ addition, we waited for the medium region clusters to self-focus until only one major peak (**4**) remained visible on the chromatograph. In experiment 1, a total of 5 additions were performed over a span of 7.6 hours. In contrast, experiment 2 involved 10 additions across a duration of 9.6 hours.

The trends of important reaction components were tracked and plotted in **Figure S39**. We plotted the trend of starting material **1** in terms of concentration, referring to its calibration curve displayed in **S2.5**. The byproduct **3** was plotted using the normalized peak area, which was calculated using the following equations:

$$Normalized\ Peak\ Area_3 = \frac{Peak\ Area_3}{Peak\ Area_{Internal\ Standard}} Average\ Peak\ Area_{Internal\ standard}$$

For small and medium region clusters, the normalized peak area shown in **Figure S 38** is calculatedby equation:

$$Normalized\ Peak\ Area_{regional\ clusters} = \frac{10\ Peak\ Area_{regional\ clusters}}{Peak\ Area_{Internal\ Standard}} Average\ Peak\ Area_{Internal\ standard}$$

A factor of 10 is used for to show the trends on the same scale.

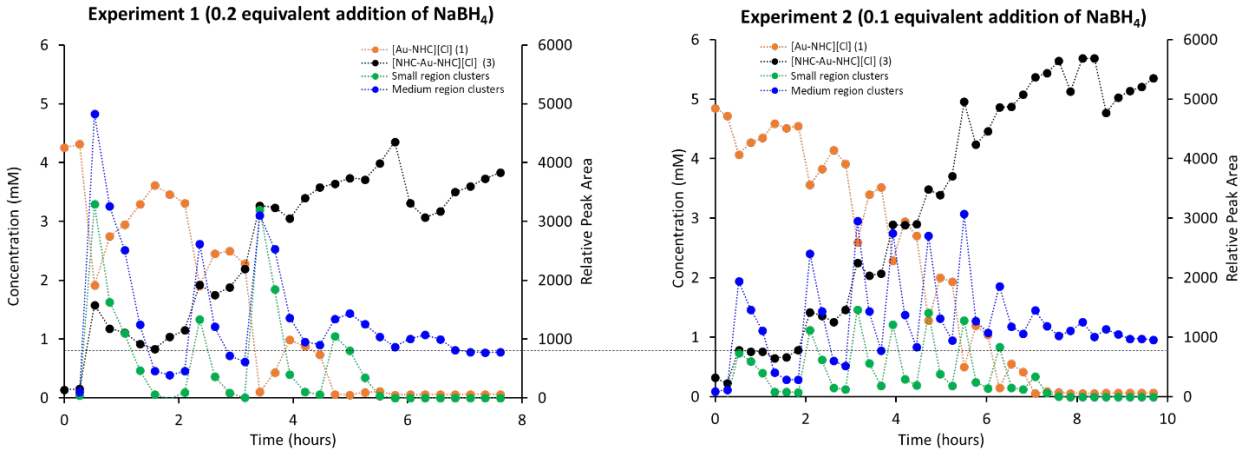

Figure S 39 Reaction monitoring trends of sequential dose experiments. Left: experiment 1 with 0.2 equivalent addition of NaBH4 solution; Right: experiment 2 with 0.1 equivalent addition of NaBH4 solution.

At the end of both of the experiments, a single peak (**4**) in medium region was remained, shown in **Figure S40**:

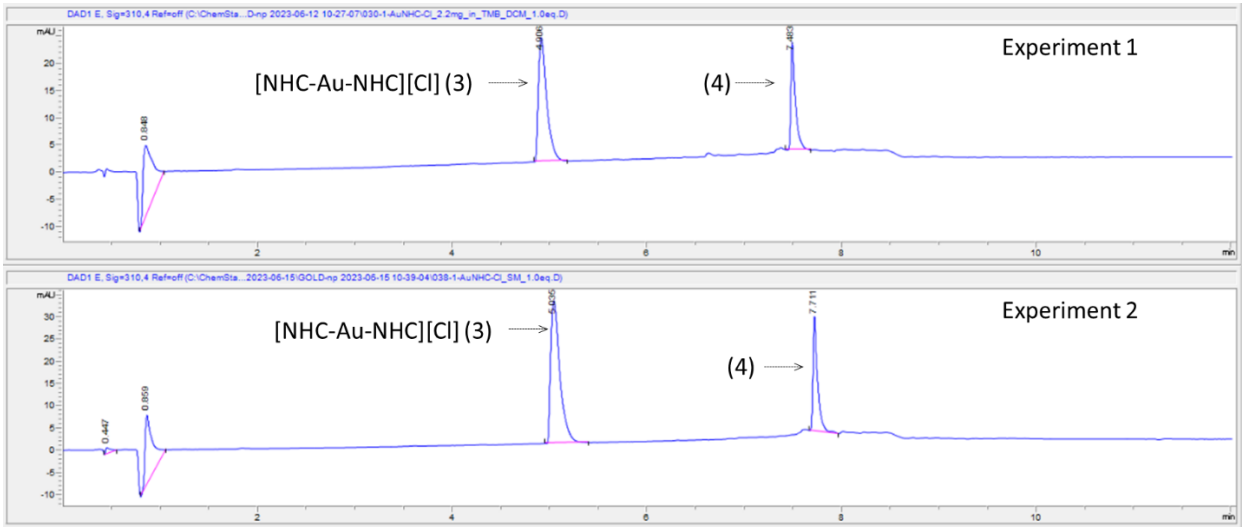

Figure S 40 Chromatograph of the last sample of experiment 1 and experiment 2. Single peak representing **4** was remained in the medium region.

As such, a comparison of the yield of product **4** between the two experiments can be done by using equation:

$$Product\ per\ starting\ material\ (\mathbf{1}) = \frac{Product\ relative\ peak\ area_{medium\ clusters}}{Starting\ material\ (\mathbf{1})_{Initial}}$$

The result of the yield comparison is listed in **Tabl S 8** below:

Table S 8 Yield comparison between experiment 1 and experiment 2

Reaction	Final sample product relative peak area	Initial sample starting material concentration	Product peak area per starting material	Increase
Experiment 1	775.9	4.31 mM	180.02	n.a.
Experiment 2	954.9	4.72 mM	202.3	12%

Thus, the experiment with a slower addition rate (Experiment 2) showed a marginally higher yield compared to Experiment 1, with an increase of 12%. However, this improvement pales in comparison to the results reported by Zheng et al.,[8] where a yield improvement of over 50% was achieved by reducing the loading of $NaBH_4$. Our results indicate that while a slower addition rate can enhance yield, the improvement is relatively modest and may not significantly impact the overall efficiency of the process.

S8. Characterization

S8.1. [NHC-Au-MeCN]$^+$

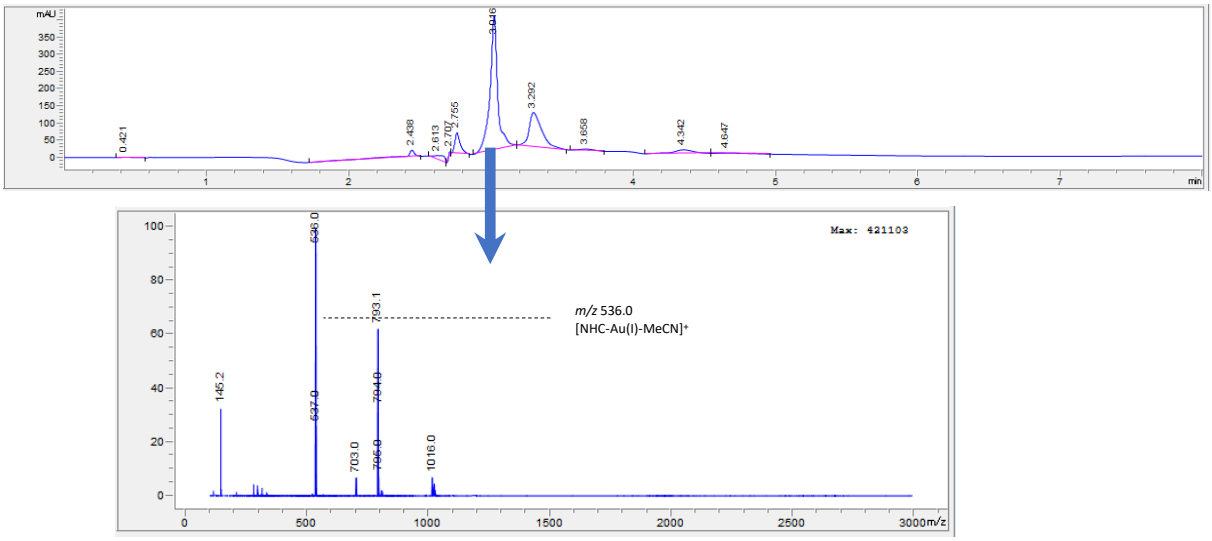

Figure S 41. HPLC chromatogram with a water/acetonitrile gradient with 0.1 % formic acid (top, the same chromatogram as Figure 1C) and the detected mass for the peak at 3.02 min (bottom), indicating the presence of [NHC-Au MeCN]$^+$ in the LC, as determined by coupled ESI-MS with an *m/z* of 536.0.

S8.2. $[Au_{13}(NHC)_9Cl_3]Cl_2$ (4)

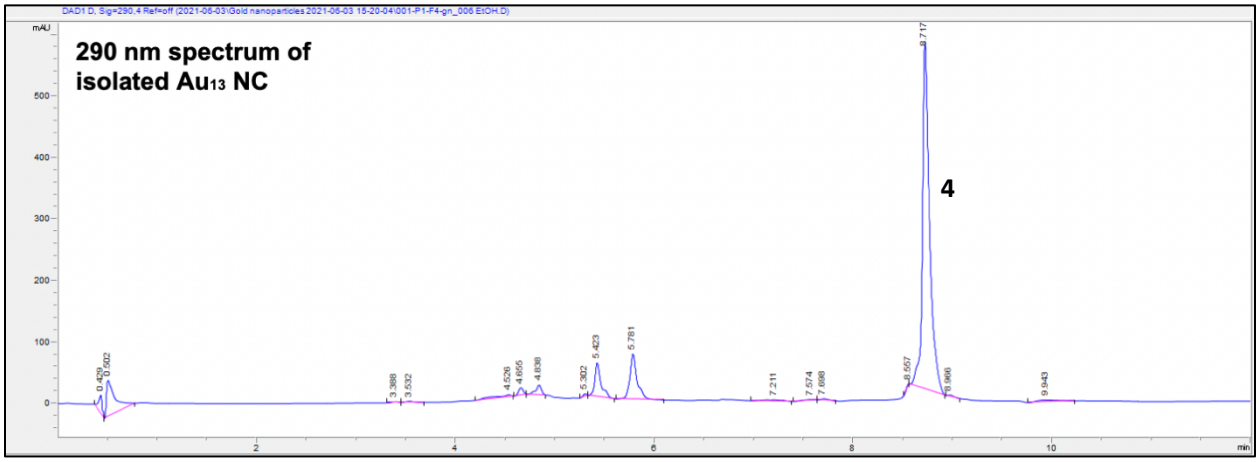

Figure S 42. HPLC spectrum of isolated $[Au_{13}(NHC)_9Cl_3]Cl_2$ detected at 290 nm

S8.3. NMR spectra

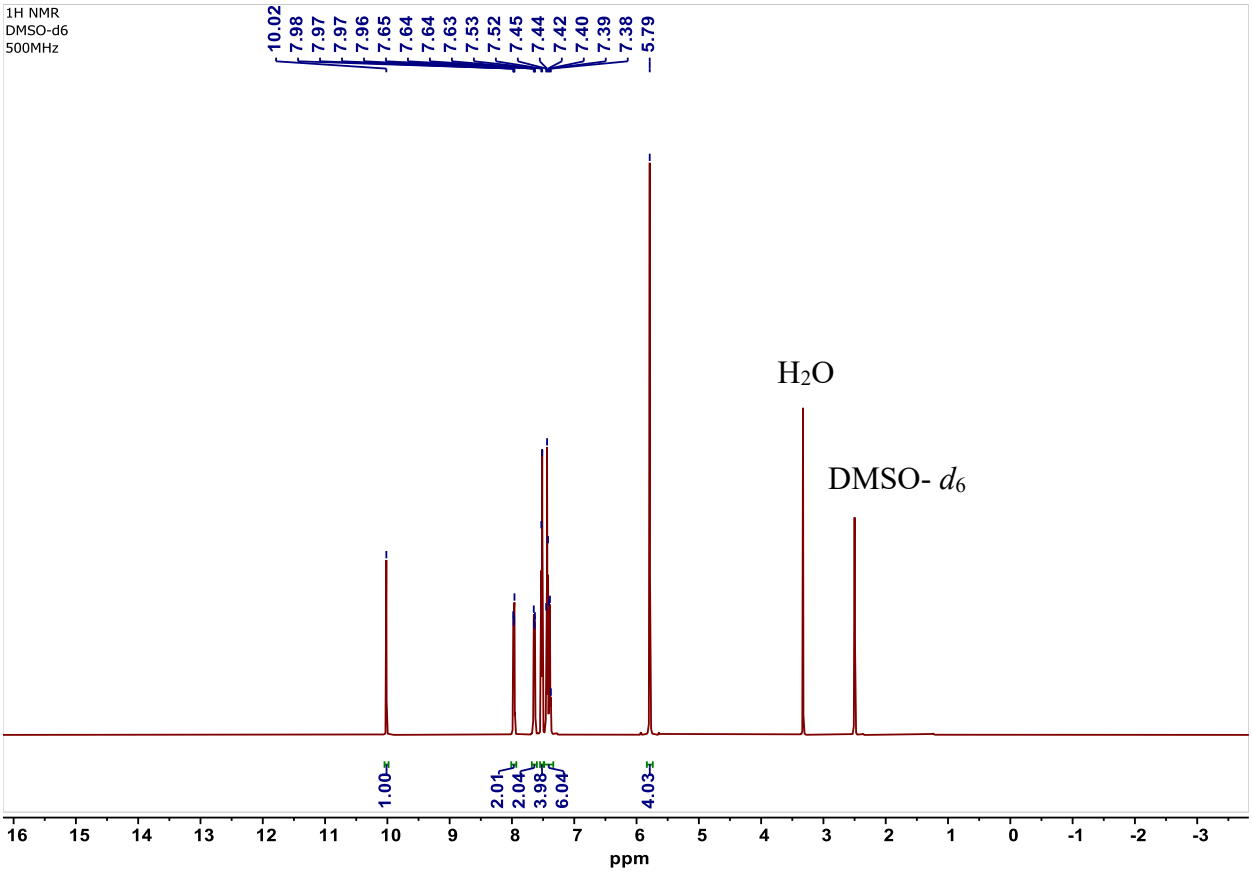

Figure S 43. ^{1}H NMR spectrum of *N,N*'-dibenzylbenzimidazolium hexafluorophosphate (DMSO- d_6, 500 MHz).

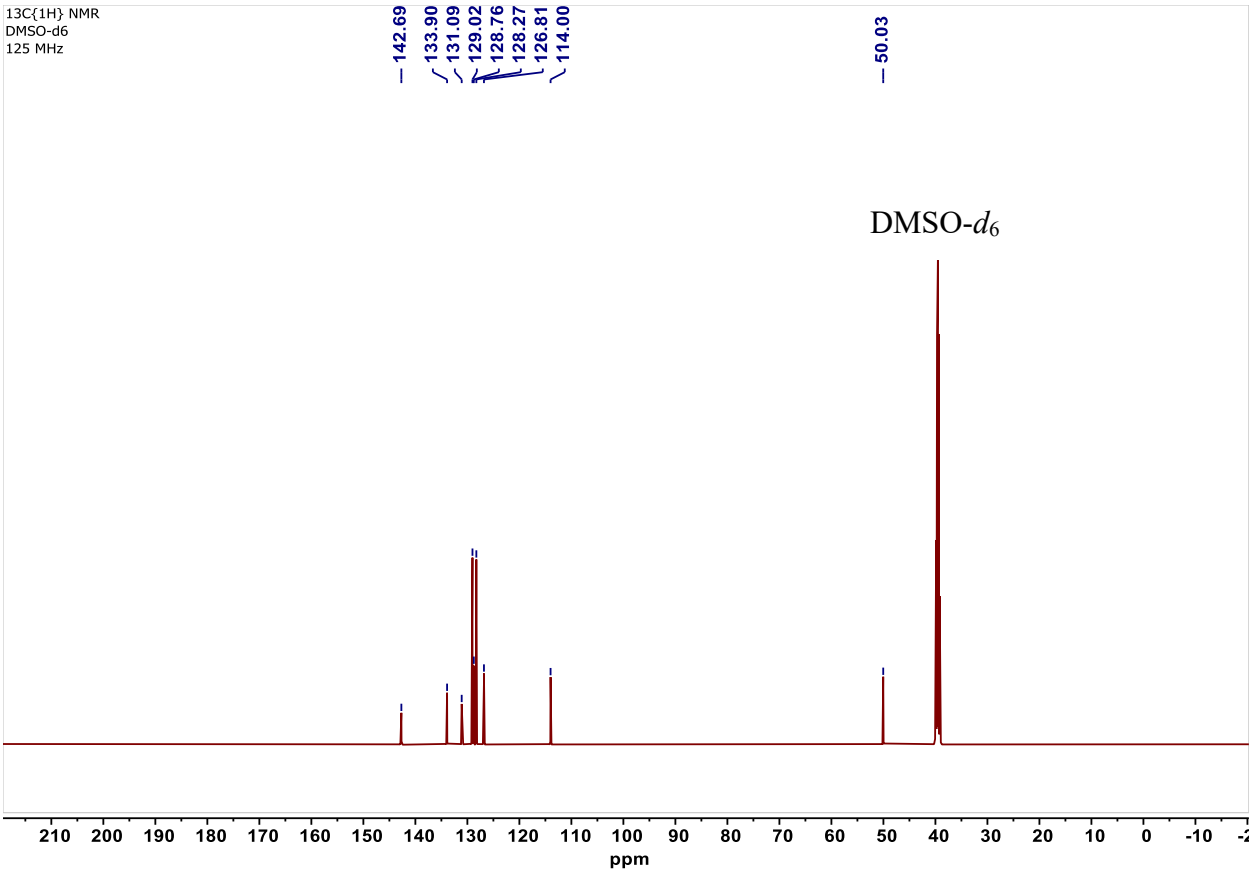

Figure S 44. $^{13}C\{^{1}H\}$ NMR spectrum of *N,N*'-dibenzylbenzimidazolium hexafluorophosphate (DMSO-d_6, 125 MHz).

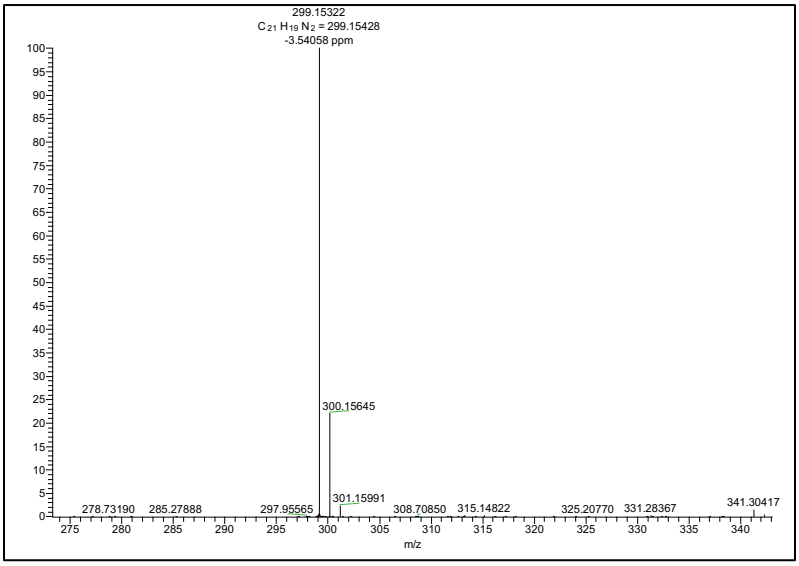

Figure S 45. Positive mode ESI-MS of *N,N*'-dibenzylbenzimidazolium hexafluorophosphate

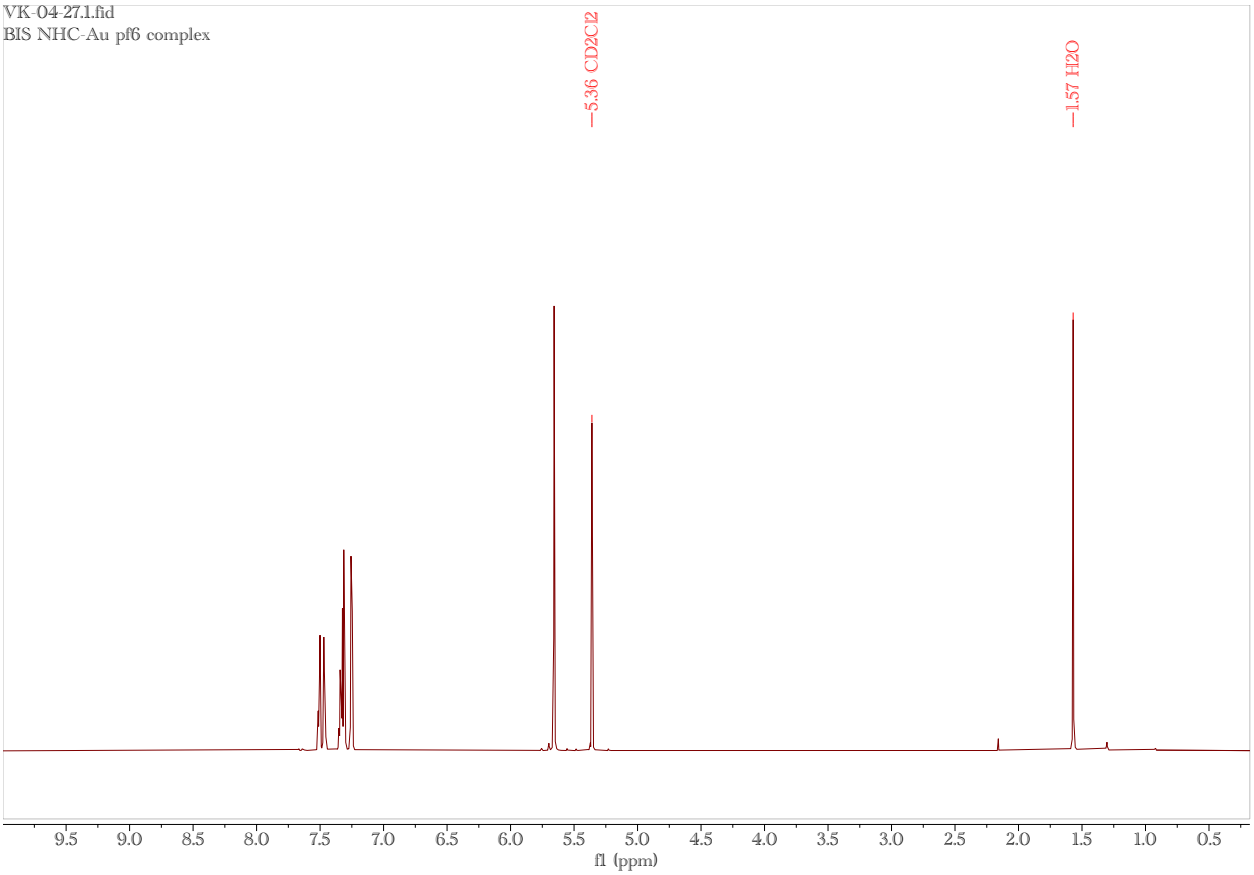

Figure S 46. ^{1}H NMR of bis(*N,N*'-dibenzylbenzimidazolium)gold hexafluorophosphate (CD_2Cl_2, 500 MHz).

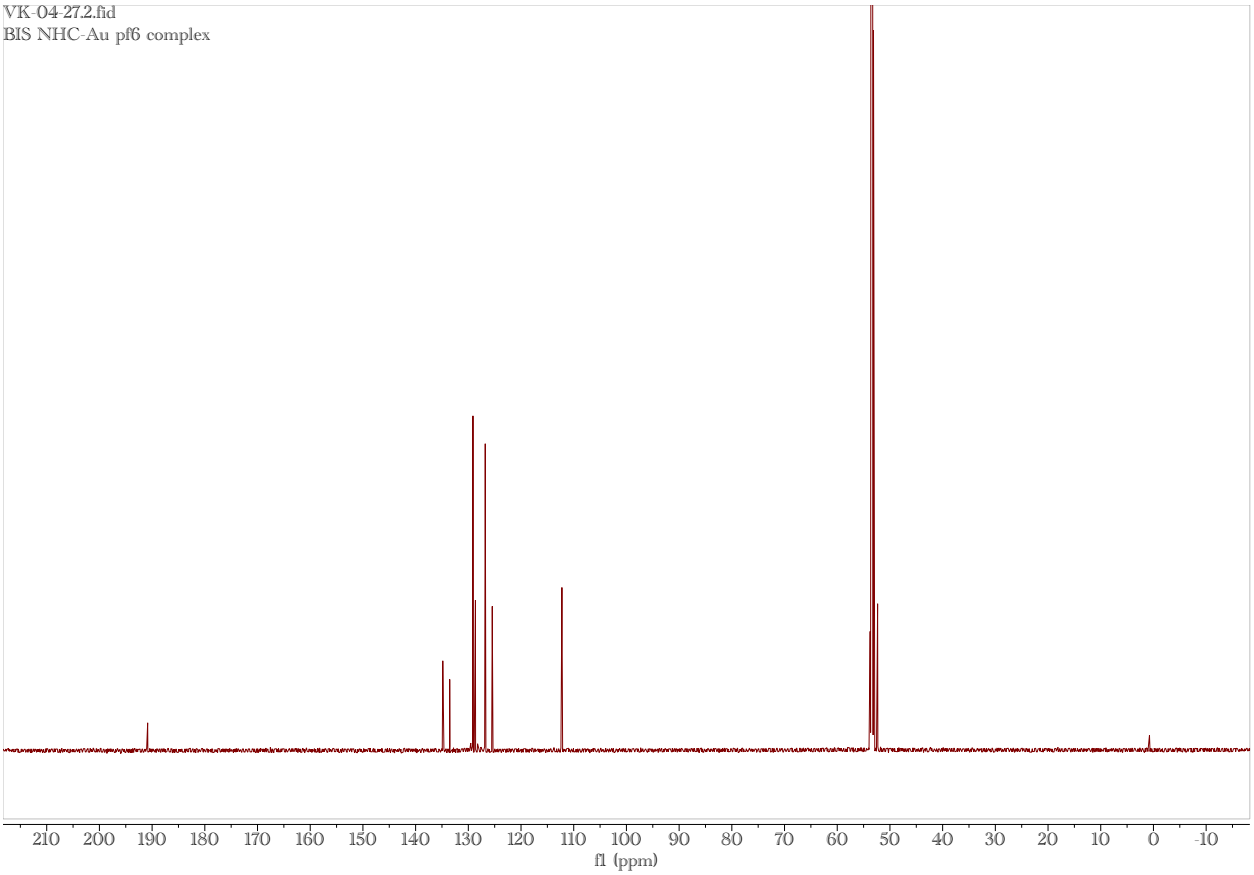

Figure S 47. $^{13}C\{^{1}H\}$ NMR spectrum of bis(*N,N*'-dibenzylbenzimidazolium)gold hexafluorophosphate (CD_2Cl_2, 125 MHz).

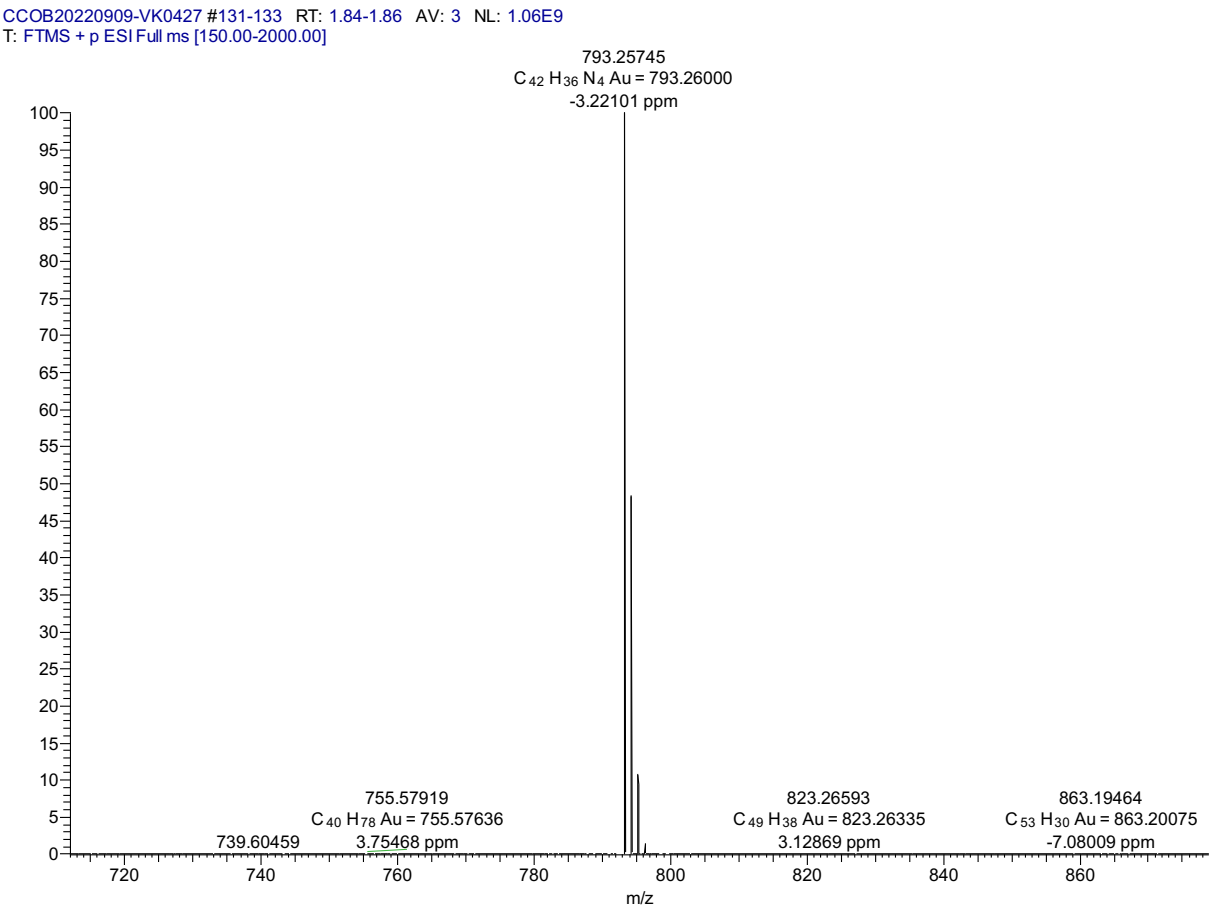

Figure S 48. Positive mode ESI-MS of bis(*N,N*'-dibenzylbenzimidazolium)gold hexafluorophosphate

S8.4. HRMS data

A reaction aliquot taken during the synthesis of $[Au_{13}(NHC)_9Cl_3]Cl_2$ (**4**) was analyzed by LC-HRMS (ESI-TOF) to support the assignment of some key ions.

m/z = 1517 $[Au_3NHC_3MeOH]^+$

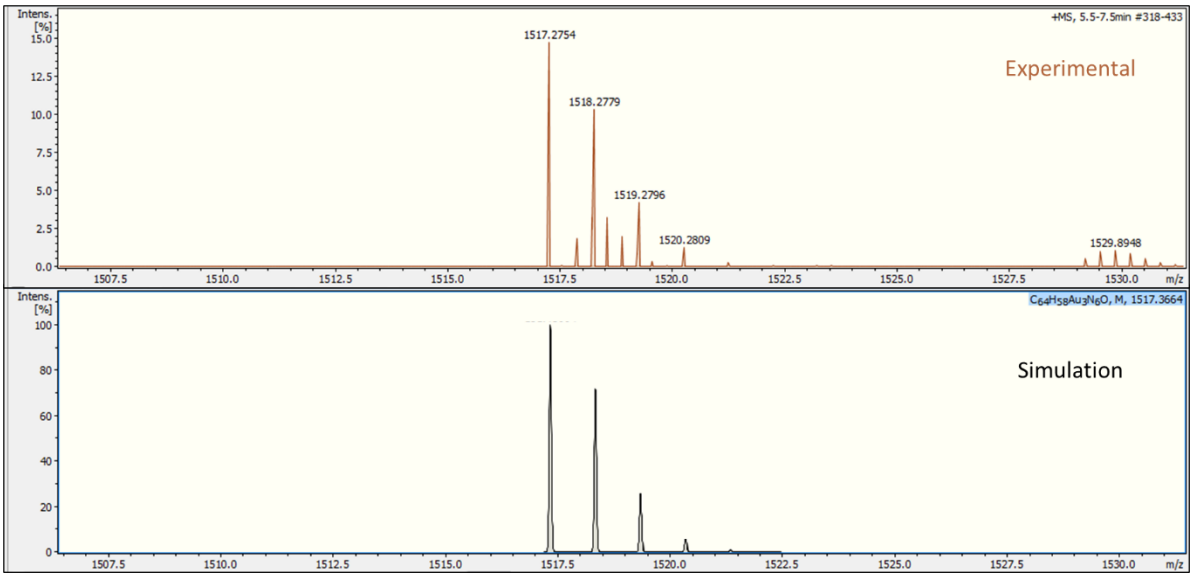

Figure S 49 Positive mode ESI-TOF of $[Au_3NHC_3MeOH]^+$

m/z = 2675 $[Au_{13}(NHC)_9Cl_3]^{2+}$

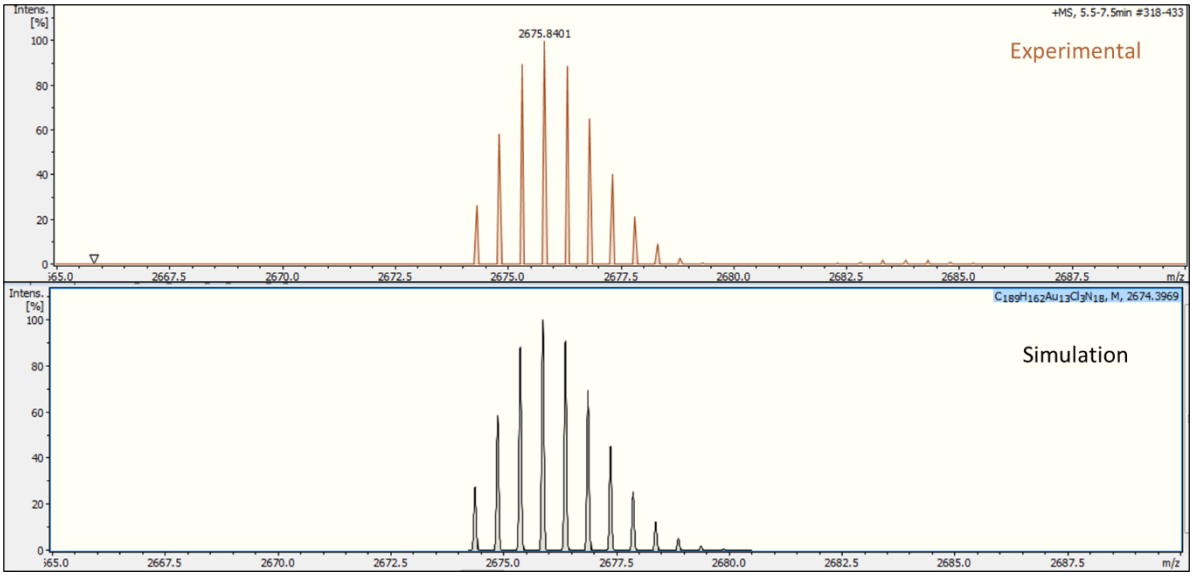

Figure S 50 Positive mode ESI-TOF of $[Au_{13}(NHC)_9Cl_3]^{2+}$

m/z = 2774 $[Au_{14}NHC_9Cl_3]^{2+}$

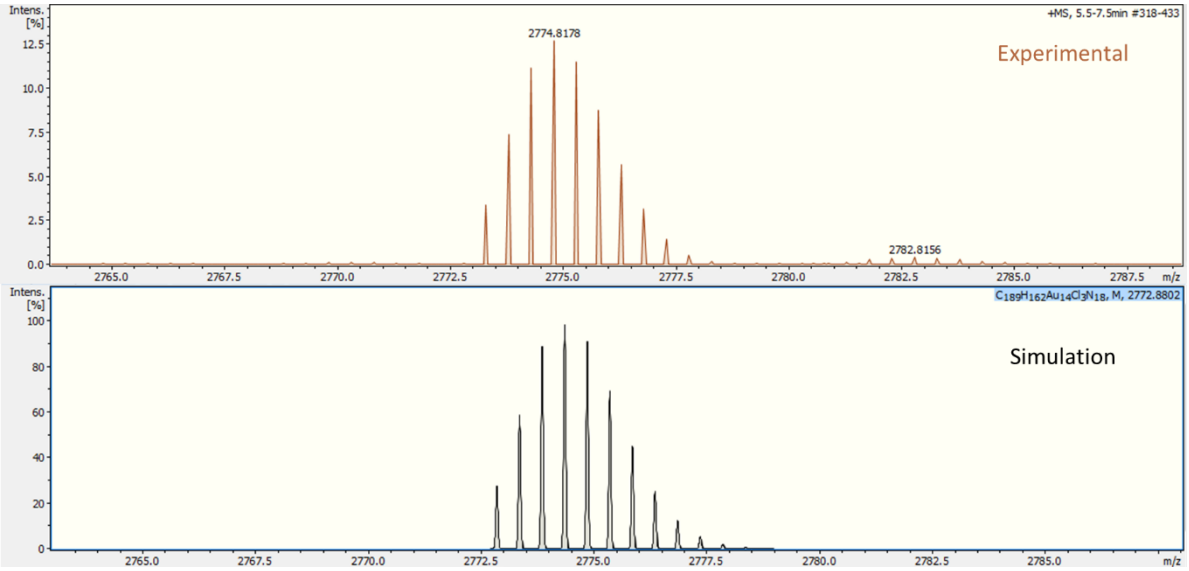

Figure S 51 Positive mode ESI-TOF of $[Au_{14}NHC_9Cl_3]^{2+}$

m/z = 2992 $[Au_{24}NHC_{14}Cl_2H_2]^{3+}$

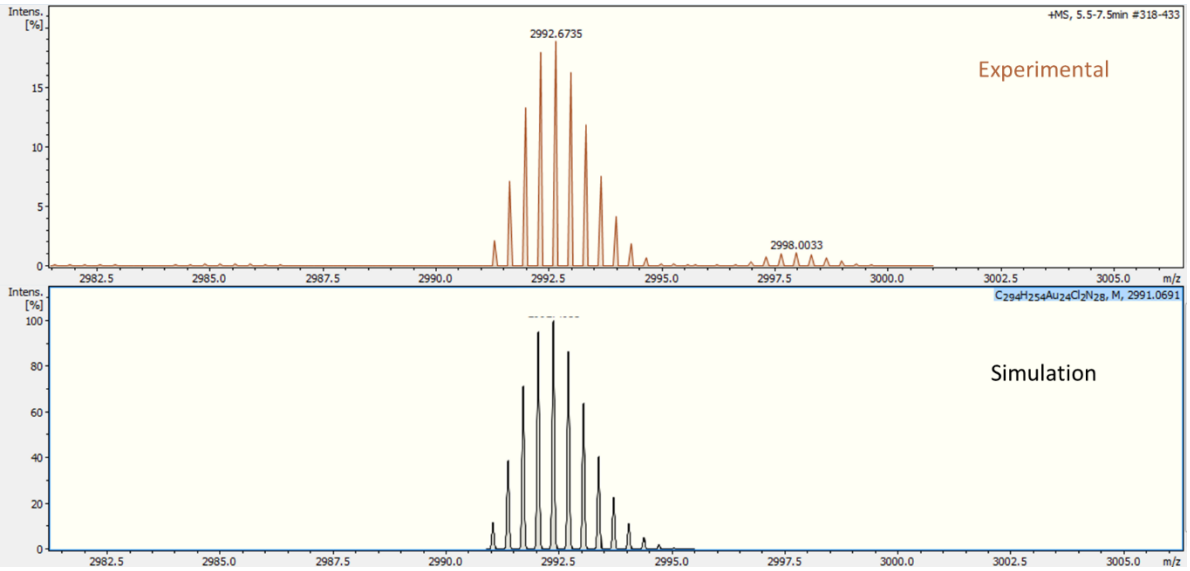

Figure S 52 Positive mode ESI-TOF of $[Au_{24}NHC_{14}Cl_2H_2]^{3+}$

S9. ^{13}C isotope NMR experiments

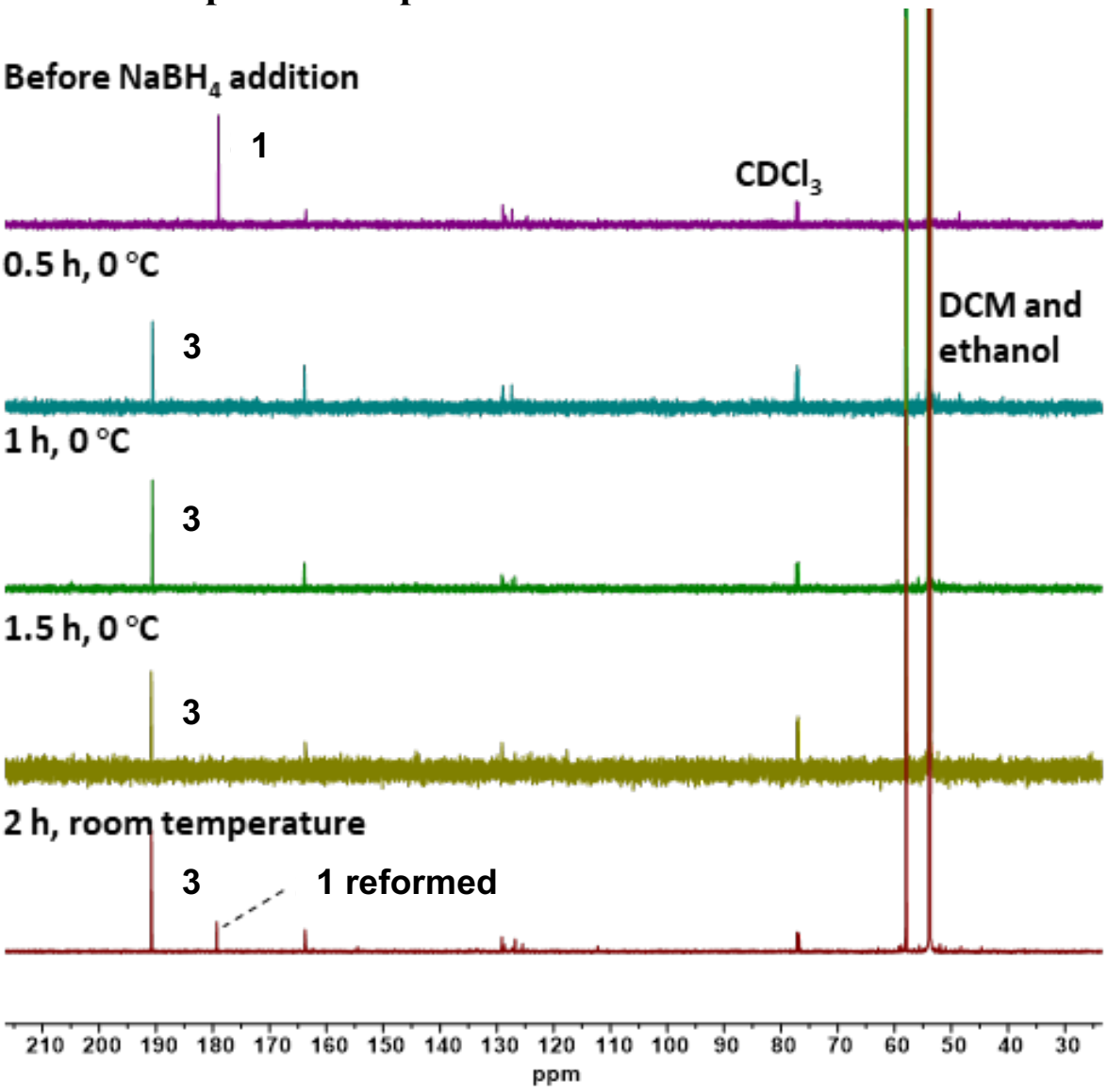

Figure S 53. 175 MHz $^{13}C\{^{1}H\}$ NMR spectra employed in monitoring of $NaBH_4$ reduction of ^{13}C-labelled 1. The spectra were acquired after dissolving 2.12 mg of 3 in 1 mL of DCM in an NMR tube. The sample was locked using a $CDCl_3$ insert and placed in an ice bath for 20 minutes before acquiring data at 273 K. Next, 40 µL of a 20 mM $NaBH_4$ solution in ethanol (1 equiv.) was added to the NMR tube and the sample was inverted and placed back into the spectrometer for reaction monitoring. Two and three minute-duration scans were continually acquired over a 90 minute period at 273 K. After 90 minutes, the sample was warmed to 298 K in the spectrometer, and the reaction was monitored. Before reaction, only the 179 ppm signal attributed to the carbene carbon in ^{13}C-labelled 3 was observed. Following addition of $NaBH_4$, the gold complex was completely consumed, and no labelled carbons were visible in the $^{13}C\{^{1}H\}$ NMR. After 5 minutes, the bis-complex 3 (191 ppm) and an unknown by-product (164 ppm) were observed. Clusters were not obserbed due to their inherently low signal/noise, which would

have required that we acquire data over a much longer time. Over the 90 minutes of the reaction, the amount of bis-complex increases. The NMR tube was warmed to room temperature, and 45 min later, the gold chloride complex (179 ppm) reappeared in the spectrum.

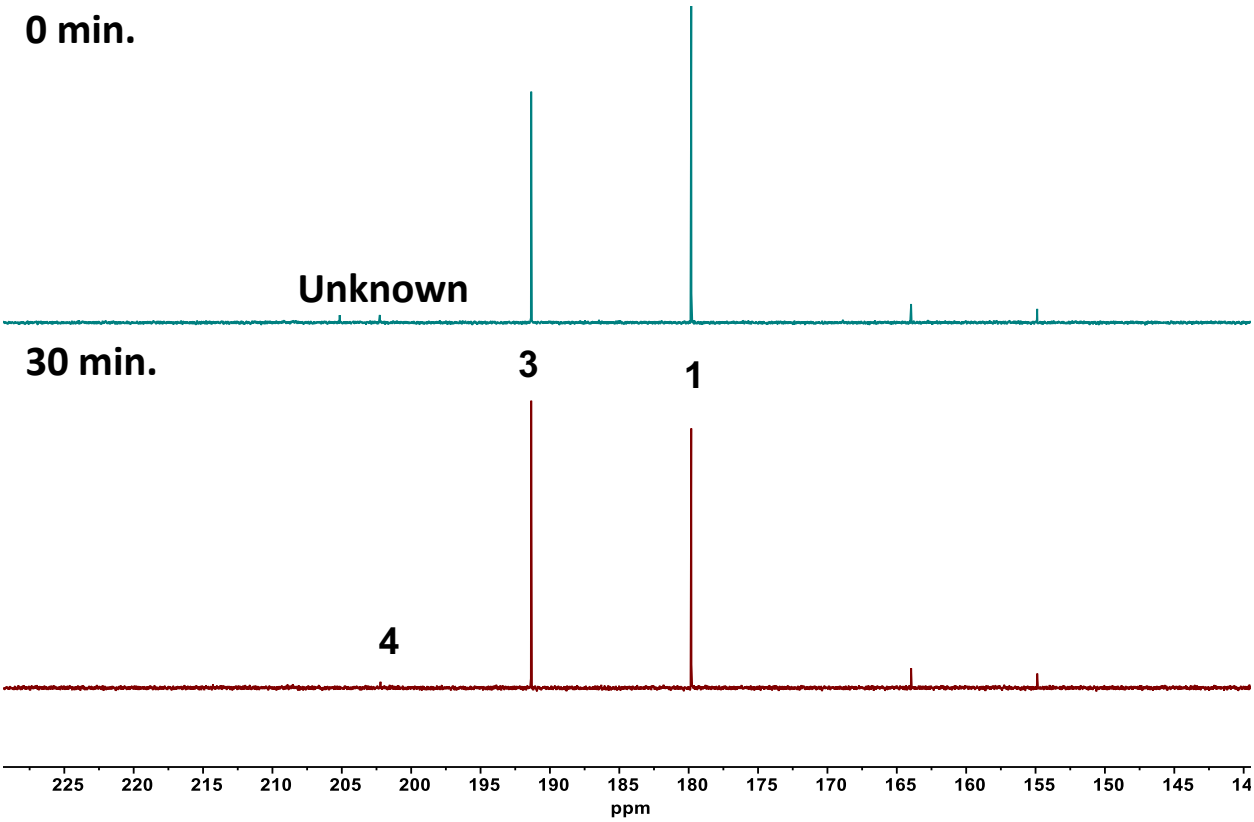

Figure S 54. 175 MHz $^{13}C\{^{1}H\}$ NMR monitoring of $NaBH_4$ reduction of ^{13}C-labelled 1. Conditions for the reaction carried out during HPLC-MS experimentation were replicated. A one dram vial was charged with 2.12 mg of 1, which was then dissolved in 1 mL of DCM. The vial was placed in an ice bath for 20 minutes. A 20 mM solution of $NaBH_4$ in ethanol 40 µL (1 equiv.) was added to the vial while stirring. In order to achieve sufficient signal/noise for the $^{13}C\{^{1}H\}$ NMR study, these reactions were performed in duplicate and combined for NMR analysis. For the sample taken at 0 minutes, the reaction mixture was immediately filtered through a PTFE syringe into a 4-dram vial and the solvent was removed *in vacuo* over 2 minutes. For the sample taken at 30 minutes, the same steps were taken after 30 minutes of stirring. The samples were then dissolved in CD_2Cl_2, and ^{13}C NMR spectroscopy performed at 298 K with long relaxation times (D1 = 15 s) to enable the detection of cluster species. An unknown cluster or clusters with chemical shifts of 202 ppm and 205 ppm was/were formed immediately upon the addition of $NaBH_4$. After 30 minutes, no signals were seen in this area and the signal for cluster 4 was detected.

References

1 M. R. Narouz, S. Takano, P. A. Lummis, T. I. Levchenko, A. Nazemi, S. Kaappa, S. Malola, G. Yousefalizadeh, L. A. Calhoun, K. G. Stamplecoskie, H. Häkkinen, T. Tsukuda and C. M. Crudden, *J. Am. Chem. Soc.*, 2019, **141**, 14997–15002.

2 V. K. Kulkarni, B. N. Khiarak, S. Takano, S. Malola, E. L. Albright, T. I. Levchenko, M. D. Aloisio, C. Dinh, T. Tsukuda, H. Häkkinen and C. M. Crudden, *J. Am. Chem. Soc.*, 2022, **144**, 9000–9006.

3 G. R. Fulmer, A. J. M. Miller, N. H. Sherden, H. E. Gottlieb, A. Nudelman, B. M. Stoltz, J. E. Bercaw and K. I. Goldberg, *Organometallics*, 2010, **29**, 2176–2179.

4 S. Misra, M. F. Wahab, D. C. Patel and D. W. Armstrong, *J. Sep. Sci.*, 2019, **42**, 1644–1657.

5 J. F. DeJesus, L. M. Sherman, D. J. Yohannan, J. C. Becca, S. L. Strausser, L. F. P. Karger, L. Jensen, D. M. Jenkins and J. P. Camden, *Angew. Chemie Int. Ed.*, 2020, **59**, 7585–7590.

6 I. Maisuls, F. Boisten, M. Hebenbrock, J. Alfke, L. Schürmann, B. Jasper-Peter, A. Hepp, M. Esselen, J. Müller and C. A. Strassert, *Inorg. Chem.*, 2022, **61**, 9195–9204.

7 R. Jothibasu, H. V. Huynh and L. L. Koh, *J. Organomet. Chem.*, 2008, **693**, 374–380.

8 H. Shen, X. Tang, Q. Wu, Y. Zhang, C. Ma, Z. Xu, B. K. Teo and N. Zheng, *ACS Nanosci. Au*, 2022, **2**, 520–526.